Free Radical Biology and Medicine 72 (2014) 41–54

Contents lists available at ScienceDirect

Free Radical Biology and Medicine

journal homepage: www.elsevier.com/locate/freeradbiomed

Original Contribution

Dimerization of visinin-like protein 1 is regulated by oxidative stress and calcium and is a pathological hallmark of amyotrophic lateral sclerosis

Martina P. Liebl [a], Ali M. Kaya [a], Stefan Tenzer [b], Romy Mittenzwei [a], Ingrid Koziollek-Drechsler [a], Hansjörg Schild [b], Bernd Moosmann [a], Christian Behl [a], Albrecht M. Clement [a,*]

[a] Institute for Pathobiochemistry, University Medical Center, Johannes Gutenberg University, D-55099 Mainz, Germany
[b] Institute for Immunology, University Medical Center, Johannes Gutenberg University, D-55099 Mainz, Germany

ARTICLE INFO

Article history:
Received 14 February 2014
Received in revised form
4 April 2014
Accepted 5 April 2014
Available online 15 April 2014

Keywords:
VILIP-1
Amyotrophic lateral sclerosis
Cysteine
Redox sensor
Free radicals

ABSTRACT

Redox control of proteins that form disulfide bonds upon oxidative challenge is an emerging topic in the physiological and pathophysiological regulation of protein function. We have investigated the role of the neuronal calcium sensor protein visinin-like protein 1 (VILIP-1) as a novel redox sensor in a cellular system. We have found oxidative stress to trigger dimerization of VILIP-1 within a cellular environment and identified thioredoxin reductase as responsible for facilitating the remonomerization of the dimeric protein. Dimerization is modulated by calcium and not dependent on the myristoylation of VILIP-1. Furthermore, we show by site-directed mutagenesis that dimerization is exclusively mediated by Cys187. As a functional consequence, VILIP-1 dimerization modulates the sensitivity of cells to an oxidative challenge. We have investigated whether dimerization of VILIP-1 occurs in two different animal models of amyotrophic lateral sclerosis (ALS) and detected soluble VILIP-1 dimers to be significantly enriched in the spinal cord from phenotypic disease onset onwards. Moreover, VILIP-1 is part of the ALS-specific protein aggregates. We show for the first time that the C-terminus of VILIP-1, containing Cys187, might represent a novel redox-sensitive motif and that VILIP-1 dimerization and aggregation are hallmarks of ALS. This suggests that VILIP-1 dimers play a functional role in integrating the cytosolic calcium concentration and the oxidative status of the cell. Furthermore, a loss of VILIP-1 function owing to protein aggregation in ALS could be relevant in the pathophysiology of the disease.

In addition to the detrimental damage to biomolecules mediated by reactive oxygen species (ROS)[1], oxidative modifications by distinct ROS such as hydrogen peroxide (H_2O_2) regulate protein structure and function in a physiological manner [1]. One of these modifications is the formation of inter- and intramolecular disulfide bonds of cytosolic proteins that serve as redox sensors and regulate a wide range of cellular processes. Among those are transcription factors such as Yes-associated protein 1 (Yap1) [2], molecular chaperones, and translation factors, as well as proteins involved in energy metabolism, signal transduction, and apoptosis [3]. However, relatively little is known about the nature of regulatory cysteine sites in proteins and whether these sites share any common characteristics [4].

Members of the neuronal calcium sensor (NCS) protein family, such as visinin-like protein 1 (VILIP-1), possess highly conserved cysteine residues. These proteins are predominantly neuronally expressed calcium sensors belonging to the superfamily of EF-hand calcium-binding proteins that are involved in a variety of cellular processes [5]. Many members of the NCS protein family perform a so-called calcium–myristoyl switch upon calcium binding, releasing the myristoyl residue from a hydrophobic pocket inside the protein and thus allowing the relocation of the protein from the cytosol to cellular membranes [6–8]. VILIP-1 belongs to the visinin-like protein subfamily (class B) of the NCS family, which overall comprises 14 genes [9]. It is extraordinarily conserved from zebrafish to human, indicating that this protein has a crucial function in vertebrates. VILIP-1 is 191 amino acids long and

Abbreviations: ALS, amyotrophic lateral sclerosis; AMPA, α-amino-3-hydroxy-5-methyl-4-isoxazolpropionic acid; BAPTA, 1,2-bis(2-aminophenoxy)ethane-*N*,*N*,*N*,*N*-tetraacetic acid tetrakis acetoxymethyl ester; DAPI, 4′,6′-diamidino-2-phenylindole; HEK, human embryonic kidney; hSOD1, human superoxide dismutase 1; MG-132, carbobenzoxy-l-leucyl-l-leucyl-l-leucinal; MTT, 3-(4,5-dimethylthiazole-2-yl)-2,5-diphenyltetrazolium bromide; NCS, neuronal calcium sensor; Q-TOF, quadrupole time-of-flight; ROS, reactive oxygen species; TDP-43, transactivation response DNA-binding protein of 43 kDa; TRXR, thioredoxin reductase; VILIP-1, visinin-like protein 1

* Corresponding author. Fax: +49 6131 3925792.
E-mail address: clement@uni-mainz.de (A.M. Clement).

http://dx.doi.org/10.1016/j.freeradbiomed.2014.04.008

binds two calcium ions [10] in a cooperative manner, with calcium binding first to the high-affinity EF-hand 3 binding site and subsequently to the EF-hand 2 binding site [11]. VILIP-1 possesses three cysteine residues at positions Cys38, Cys87, and Cys187, with Cys87 being present exclusively in VILIP-1 and VILIP-2, and not in other class B family members. Based on data from in vitro experiments, it is controversial whether VILIP-1 is able to dimerize by covalent interactions and whether calcium binding triggers dimer formation [11–13].

VILIP-1 has been shown to be involved in a variety of cellular functions. There is compelling evidence that VILIP-1 is involved in clathrin-dependent receptor trafficking and exocytosis by modulating the surface expression of transmembrane receptors, thereby increasing cellular cGMP and cAMP levels [14–20]. VILIP-1 was also described to bind double-stranded RNA [21] and has been shown to act as a tumor suppressor by inhibiting cell proliferation and migration [22–24]. Furthermore, there is evidence that VILIP-1 is involved in long-term potentiation and synaptic plasticity [25]. Altered VILIP-1 expression and localization have been described in Alzheimer disease (AD) and schizophrenia [26–28]. Moreover, downregulation of VILIP-1 has been reported in amyotrophic lateral sclerosis (ALS) [29].

ALS is a progressive, late-onset neurodegenerative disease leading to the loss of motor neurons in the spinal cord, the brain stem, and the motor cortex. It is characterized by intracellular protein aggregates, glial activation, mitochondrial dysfunction, and perturbed calcium homeostasis. The increased presence of ROS in the course of disease owing to misregulation of NADPH oxidases, mitochondrial damage, and downregulation of antioxidative enzymes has been determined as one of the prominent cytotoxic components in ALS [30–32]. In addition, calcium homeostasis within motor neurons is particularly susceptible to insult because of low levels of calcium binding proteins [33–35]. An increased calcium uptake induced by elevated extracellular glutamate levels, which are caused by reduced astrocytic glutamate uptake [36–39] and by AMPA receptors lacking the GluR2 subunit [40,41], results in excitotoxicity. This detrimental process is at least partially mediated by an increased uptake of calcium into mitochondria, which in turn results in elevated ROS production [42,43], indicating that oxidative stress and excitotoxicity enhance each other to contribute to ALS pathology [44].

Here, we investigated whether VILIP-1 represents an oxidative stress sensor in cells as well as in animal models of ALS. By site-directed mutagenesis we provide evidence that VILIP-1 undergoes reversible oxidative stress-induced dimerization that is mediated by Cys187. We found dimerization of VILIP-1 to strongly depend on calcium, but not on protein relocation due to its myristoyl residue. By employing survival assays we analyzed the impact of VILIP-1 dimerization and myristoylation on the sensitivity of cells to an oxidative challenge. Finally, the analysis of tissues from two different rodent models of ALS showed that VILIP-1 dimer formation correlates with disease progression. Based on our data we propose that VILIP-1 is a redox sensor that integrates Ca^{2+} homeostasis and the level of oxidative stress within a cell. Furthermore, the presence of disease-related VILIP-1 dimers and aggregates points to a possible role of VILIP-1 in the progression of motor neuron disease.

Materials and methods

Animals

Mice were kept in the animal facility of the University Medical Center (ZVTE) and were housed, anesthetized, and sacrificed according the state law of Rheinland-Pfalz and European and German guidelines for the care and use of laboratory animals. Mice overexpressing human wild-type SOD1 ($hSOD1^{WT}$; B6/SJFL/TgN(SOD1)-2Gur), the $hSOD1^{G93A}$ mutant with low copy number ($hSOD1^{G93A}$; B6/SJL/TgN(SOD1-G93A)-Gur) (The Jackson Laboratory, Bar Harbor, ME, USA), and the human $SOD1^{G85R}$ ($hSOD^{G85R}$) mutant were kept hemizygous, and nontransgenic littermates served as controls. Disease onset was defined when the maximum body weight was reduced by 10% (260 and 331 days of age for $hSOD1^{G93A}$ and $hSOD1^{G85R}$, respectively). End stage of disease was defined as when the mice were not able to right themselves up within 10 s when laid on the side (298 and 369 days of age for $hSOD1^{G93A}$ and $hSOD1^{G85R}$, respectively). Owing to the differences in survival of $hSOD1^{G93A}$ and $hSOD1^{G85R}$ transgenic mice, presymptomatic mice were analyzed at 4 and 7 months of age, respectively.

Spinal cord tissues from hSOD1 transgenic rats were kindly provided by Drs. S. Boillee and C. Lobsiger (Paris, France).

Generation of VILIP-1 constructs

VILIP-1 without green fluorescent protein (GFP) was amplified from a plasmid carrying the human wild-type VILIP-1–GFP ($VILIP\text{-}1^{WT\text{-}GFP}$) in pEGFPN1 (gift from Professor K.H. Braunewell, Birmingham, AL, USA) with primers spanning the BglII and SalI restriction sides (see Supplementary Table 1) and ligated into a modified pEGFP-N1 (Clontech) vector without EGFP (pN1). From this vector, VILIP-1 without GFP was inserted into the pEF-BOS-EX vector (gift from Professor S. Nagata, Kyoto, Japan [45,46]) using the NheI and the SalI restriction sides.

Point mutations (G2A, C38A, C87A, C187A) were inserted into $VILIP\text{-}1^{WT}$ in pEF-BOS-EX using the Quick Change Lightning site-directed mutagenesis kit (Agilent Technologies). The sequences of suitable forward and reverse primers for mutagenesis can be viewed in Supplementary Table 2. To ensure correct insertion of the point mutations, the plasmids were sequenced (Genterprise, Mainz, Germany).

Cell culture

Human embryonic kidney cells 293 A (HEK293A) were cultivated on plastic dishes with Dulbecco's modified Eagle's medium (DMEM; Life Technologies) supplemented with fetal calf serum (10%), 1% sodium pyruvate (Life Technologies), and antibiotics. Cells were cultivated at 37 °C in a humidified atmosphere containing 5% CO_2. For transient transfection the calcium phosphate precipitation method was applied, which is detailed in the supplementary material.

In the case of short-term incubations (2 to 90 min), H_2O_2, diamide, *N*-acetylcysteine, auranofin, ionomycin (all from Sigma–Aldrich), MG-132 (Calbiochem), or BAPTA (Life Technologies) was added in the appropriate concentration directly into the medium 48 h posttransfection and incubated for the indicated time intervals. In the case of overnight preincubation with auranofin, the substance was added to the medium 24 h after transfection after washing the cells. Dishes were placed on ice and washed twice with phosphate-buffered saline (PBS) before harvest. Cell pellets were stored at −80 °C until homogenization.

For recovery experiments cells were incubated with H_2O_2 or vehicle for 2 min. Subsequently, the cells were either harvested or washed twice with DMEM and supplemented with fresh medium without H_2O_2. The cells were allowed to recover for either 30 min or 2 h. If the impact of MG-132 or auranofin on recovery was tested, cells were preincubated with the substance or vehicle for the indicated time intervals. Additionally, MG-132, auranofin, or vehicle was added to the fresh medium during recovery.

Viability assays (MTT assays)

A calcium phosphate transfection method for cell suspensions was performed. A transfection mixture containing 60 μg plasmid DNA was prepared as described above and gently mixed with 4.4 ml cell suspension containing 300,000 cells. Five thousand cells in 90 μl were plated per well in a 96-well plate. The transfection efficiency was tested in parallel experiments confirming comparable efficiency between different constructs via Western blot analysis (data not shown). Twenty-four hours after seeding, transfection medium was removed, the cells were washed with DMEM, and 90 μl of fresh medium was added. Subsequently, 10 μl of various H_2O_2 dilutions in medium was added for 18 h. In each experiment, 6 wells were treated with the same H_2O_2 concentration. Viability was evaluated by the MTT assay, which is detailed in the supplementary material.

Extraction and fractionation of cells and tissues

To analyze total lysates, HEK293A cells were sonicated for 30 s on ice in lysis buffer (100 mM NaCl, 50 mM Tris–HCl, 0.5% NP-40; pH 8.0) containing 10 mM iodoacetamide (Sigma–Aldrich) and EDTA-free protease inhibitor cocktail (Roche).

The experimental procedure performed to separate homogenates of animal tissue into a soluble and an ALS-specific aggregate fraction was described earlier [47] and is specified in the supplementary material.

SDS–PAGE and Western blotting

Cell lysates (15 μg) and tissue extracts (5 μg) were separated by SDS–PAGE on 12 or 15% polyacrylamide gels under reducing and nonreducing conditions by adding loading buffer with or without β-mercaptoethanol, respectively. Proteins were transferred to nitrocellulose membranes and specifically detected by antibodies recognizing VILIP-1 (Proteintech Europe), hSOD1 (NCL Novocastra), ubiquitin (DAKO), and tubulin (Sigma–Aldrich). Secondary antibodies binding mouse or rabbit IgG coupled to horseradish peroxidase (Dianova) were used to develop the Western blots with the LAS 3000 Intelligent Darkboxx (Fuji). Band intensities were quantified with the AIDA Image Analyzer software (Raytest). Details are described in the supplementary material.

Immunocytochemistry and microscopy

HEK293A cells were grown on glass coverslips in six-well plates and transfected with VILIP-1 constructs, washed, and treated with substances as described above. Cells were fixed (95% ethanol, 5% acetic acid) for 7 min at −20 °C, washed with PBS, and incubated with antibodies against VILIP-1 (Proteintech Europe) (1:200 in PBS with 10% fetal calf serum) for 2 h at room temperature. Cells were incubated with a cyanine-conjugated secondary antibody (anti-rabbit-Cy2; Jackson Immunoresearch Laboratories) for 1 h at room temperature. After the cells were washed, DAPI (0.5 μg/ml) was added for nuclear staining. Microscopic analysis was performed with an inverted Axiovert 200 microscope (Zeiss) equipped with a SPOT RT CCD camera from Diagnostic Instruments (Visitron).

Label-free LC–MSE mass spectrometry

Insoluble fractions of total spinal cords were prepared for subsequent analysis with label-free LC–MSE (data-independent liquid chromatography/mass spectrometry) as described earlier and specified in the supplementary material [48].

Mass spectrometric analysis of the insoluble fraction was performed with a Q-TOF tandem mass spectrometer as described in [49]. Homogenization of three spinal cords, fractionation of the lysate, and label-free mass spectrometry were performed twice for each genotype, generating two biological replicates. Each lysate was analyzed in five technical replicates and only proteins that were detected at least three times were considered for further analysis. Additionally, we regarded proteins to be enriched in an ALS-specific manner only if we found them, in both $hSOD1^{mutant}$ mouse strains ($hSOD1^{G93A}$ and $hSOD1^{G85R}$), to be enriched in the insoluble fractions by at least 50% with respect to both controls (nontransgenic, $hSOD1^{WT}$). Furthermore, only proteins fulfilling the described criteria in both biological replicates were considered.

Statistical analysis

Densitometric analyses of Western blots from two groups of interest were compared by *t* test for independent samples. Survival curves from viability assays were compared by two-way analysis of variance and an all pairwise multiple comparison procedure (Holm–Sidak method). A probability of error less than 5% ($p < 0.05$) was regarded as statistically significant and less than 1% ($p < 0.01$) as highly significant. Statistical analysis was performed with SPSS (densitometric analysis) and SigmaStat (viability assays).

Results

Oxidative stress induces dimerization of VILIP-1

As protein dimerization is a major factor controlling protein function in vivo, we aimed to investigate whether VILIP-1, which has been reported to dimerize in a cell-free system [12], could act as a novel redox sensor. We transfected HEK293A cells not expressing VILIP-1 endogenously with $VILIP\text{-}1^{WT}$ and treated them with various concentrations of H_2O_2 for various time intervals. Under nonreducing analytical conditions, we observed a significant proportion of $VILIP\text{-}1^{WT}$ to dimerize in a concentration- and time-dependent manner, corresponding to a 44-kDa band on the Western blot. Heterodimers of VILIP-1 with other proteins, which would be detectable as bands of different sizes, did not form, indicating the specificity of the homodimerization. Under reducing conditions, only a single band corresponding to monomeric $VILIP\text{-}1^{WT}$ (22 kDa) was detected (Fig. 1A). Dimerization occurred rapidly, as 2 min of oxidative stimulus significantly increased the amount of $VILIP\text{-}1^{WT}$ dimer and was further enhanced when cells were treated for up to 10 min (Fig. 1A). No morphological changes or damage of the cells were observed after these incubation intervals (Supplementary Fig. 1A). The acute induction of VILIP-1 dimers is a general response to thiol oxidative stress, as diamide also induced VILIP-1 dimerization in a dose-dependent manner (Supplementary Fig. 1B).

If the dimerization of VILIP-1 was caused by a direct oxidative effect, dimerization should be attenuated by preincubation with a thiol-based antioxidant before the oxidative challenge. To test this, we preincubated $VILIP\text{-}1^{WT}$-transfected cells with *N*-acetylcysteine before treating them with H_2O_2. We detected significantly less VILIP-1 dimer formation compared to controls not pretreated with *N*-acetylcysteine (Fig. 1B).

To control whether the band at 44 kDa refers to a VILIP-1 homodimer, we treated $VILIP\text{-}1^{WT\text{-}GFP}$ (51 kDa)-overexpressing cells with H_2O_2. Treatment of $VILIP\text{-}1^{WT\text{-}GFP}$-transfected cells with H_2O_2 indeed resulted in a specific band with a size > 100 kDa (Supplementary Fig. 1C), confirming that the observed

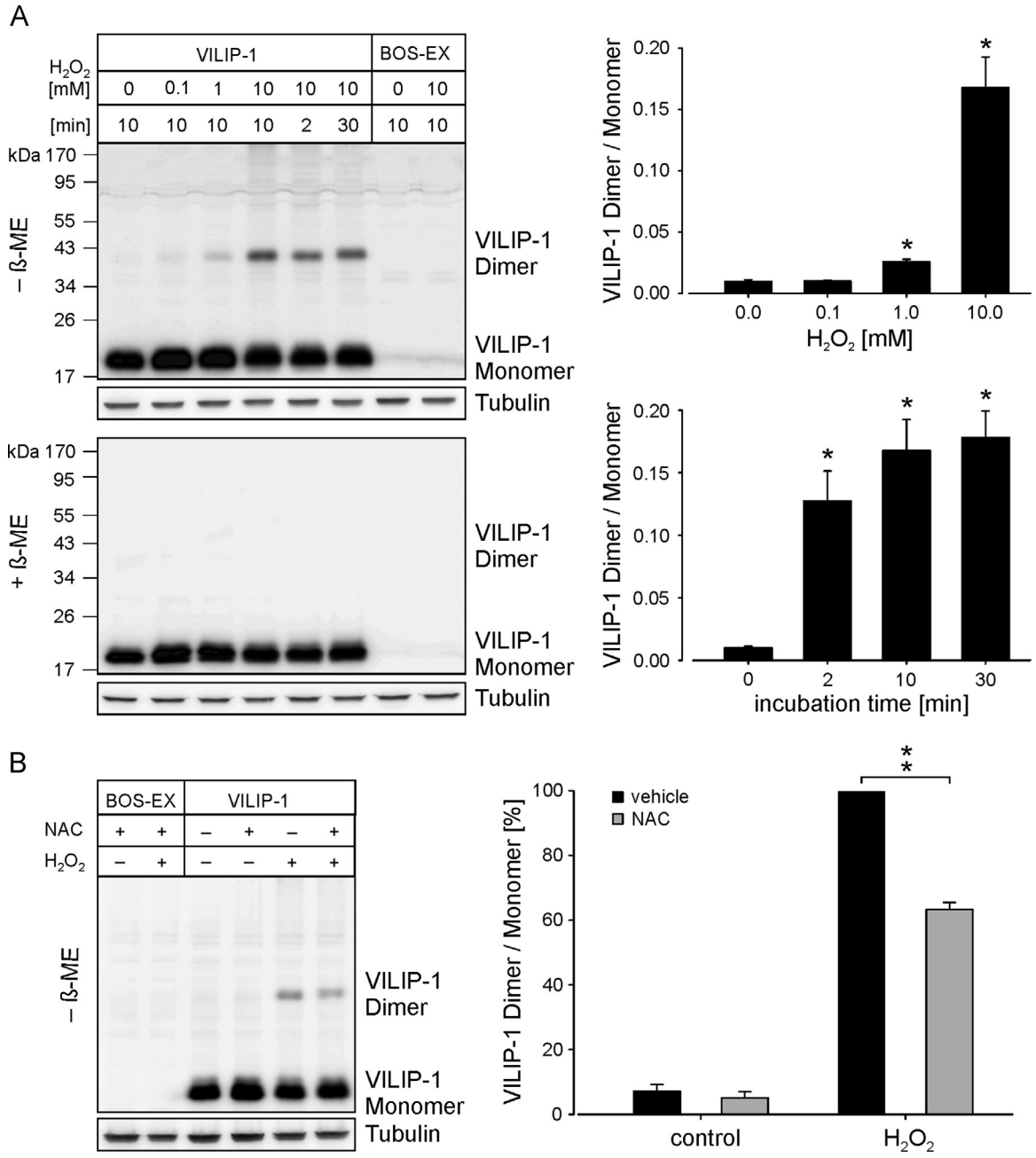

Fig. 1. Effects of oxidative stress on VILIP-1 dimerization. (A and B) VILIP-1^{WT}-transfected HEK293A cells were treated with the indicated H_2O_2 concentrations for the indicated time intervals. Cell lysis buffer was supplemented with iodoacetamide to block free SH groups of proteins to prevent dimerization of VILIP-1 during subsequent analysis. 15 μg of total protein lysate was separated under nonreducing (−β-ME) and reducing (+β-ME) conditions (not shown for (B)) on 12% polyacrylamide gels and analyzed on Western blots. To normalize for transfection efficiency, the ratio between VILIP-1 dimer and VILIP-1 monomer was calculated. (A) Ratio of VILIP-1 dimer vs monomer was plotted against various H_2O_2 concentrations (upper graph) or incubation times (lower graph). The mean ± SEM of three independent experiments is shown. Treatment with 1 or 10 mM H_2O_2 for 10 min caused significant dimerization of VILIP-1 (top). Dimerization of VILIP-1 was significant already after 2 min of incubation with 10 mM H_2O_2 and still detectable after 30 min of incubation (bottom). (B) Cells were preincubated with either 10 mM *N*-acetylcysteine (NAC) or vehicle for 1 h before adding 10 mM H_2O_2 for 10 min. The VILIP-1 dimer/monomer ratio in cells incubated with 10 mM H_2O_2 for 10 min was normalized to 100%. The mean value of four independent experiments ± SEM is shown. Dimerization of VILIP-1 was significantly reduced by preincubation with NAC. $^{*}p < 0.05$, $^{**}p < 0.01$.

modification of VILIP-1 upon oxidative challenge represents a homodimer of two VILIP-1 molecules, mediated by a disulfide bond.

Dimerization of VILIP-1 can be reversed by the thioredoxin system

If the VILIP-1 dimer acts in cellular signaling, one would expect that dimer formation is reversible. To test this, we challenged VILIP-1^{WT}-transfected cells with H_2O_2 for 2 min and allowed cells to recover for either 30 min or 2 h in H_2O_2-free medium. Thirty minutes of recovery were sufficient to reduce the amount of VILIP-1^{WT} dimer significantly, and after 2 h, the amount of VILIP-1^{WT} dimer was indistinguishable from that in untreated cells (Fig. 2).

Next we asked whether the loss of VILIP-1 dimer was either due to degradation via the proteasome or due to specific remonomerization of the dimer by a distinct cellular mechanism. To investigate the first possibility, we inhibited the proteasome with MG-132 and allowed cells to recover for 30 min in H_2O_2-free medium after oxidative stimulation. Polyubiquitinated proteins were detected as a marker for proteasome inhibition. We observed

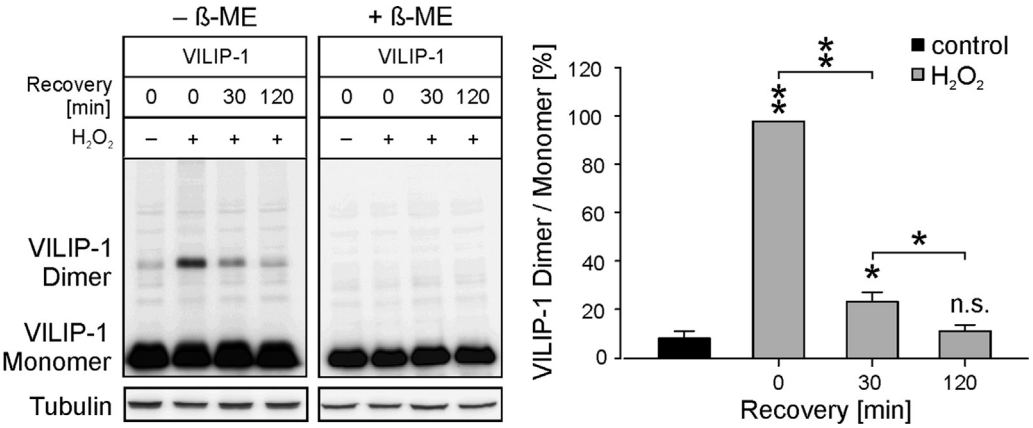

Fig. 2. VILIP-1 dimerization induced by short-term oxidative challenge is completely reversible. VILIP-1-transfected cells were treated with 10 mM H_2O_2 for 2 min and harvested directly or supplemented with fresh medium without H_2O_2 for the indicated time intervals. Total cell lysates (15 μg protein) were separated under nonreducing (−β-ME) and reducing (+β-ME) conditions on 12% SDS–polyacrylamide gels and analyzed by Western blotting. The ratios of VILIP-1 dimer vs monomer were calculated to normalize for transfection efficiency. The VILIP-1 dimer/monomer ratio after H_2O_2 treatment without recovery was set to 100%. The mean value of three independent experiments ± SEM is shown. After 2 h of recovery, the VILIP-1 dimer/monomer ratio was further reduced significantly and indistinguishable from that in control cells. Statistical significance compared to control conditions without H_2O_2 exposure: $^*p < 0.05$, $^{**}p < 0.01$.

that neither VILIP-1 dimer formation nor removal under conditions of proteasome inhibition was impaired (Fig. 3A). To investigate a thiol-dependent mechanism potentially mediating the re-monomerization of VILIP-1 dimers, the role of the thioredoxin system was analyzed. We pretreated cells with the thioredoxin reductase (TRXR) inhibitor auranofin for either 15 h or 90 min to analyze whether the removal of the VILIP-1 dimer was impaired during recovery under conditions of TRXR inhibition. Owing to auranofin treatment, an increased dimer formation upon stimulation with H_2O_2 was observed. We further found that the removal of the VILIP-1 dimer was impaired when cells had been pretreated with auranofin (Fig. 3B). Therefore, we conclude that the thior-edoxin system is involved in the remonomerization of VILIP-1 dimers in vivo, providing a cellular switch to turn off VILIP-1 dimer function when the redox environment changes to more reducing conditions.

VILIP-1 dimerization is exclusively mediated by Cys187

VILIP-1 possesses three cysteine residues. Cys38 and Cys87 are localized in the N-terminal region of the inactive EF-hand 1 and in the C-terminal part of the EF-hand 2, respectively. Cys187 is not part of an EF-hand and is localized in the C-terminus of VILIP-1 (Fig. 4A). To investigate the role of the individual cysteine residues in dimer formation, we generated point mutations for each cysteine residue, changing cysteine to alanine. We transfected cells with VILIP-1^{WT}, VILIP-1^{C38A}, VILIP-1^{C87A}, or VILIP-1^{C187A} and stimulated them with H_2O_2. We observed that VILIP-1^{C38A} and VILIP-1^{C87A} dimerization in response to oxidative stress were not altered compared to VILIP-1^{WT} dimer formation, showing that Cys38 and Cys87 are not involved in the dimerization. In the case of transfection with VILIP-1^{C187A}, no dimerization was induced by H_2O_2 (Fig. 4B). These results show that the C-terminal residue Cys187 is exclusively involved in the homodimerization of VILIP-1.

VILIP-1 dimerization is calcium-dependent, but does not require membrane localization

VILIP-1 binds two calcium ions in a cooperative manner. Calcium binding leads to the calcium–myristoyl switch of the cytosolic protein and attaches VILIP-1 to the plasma membrane and *trans*-Golgi membranes [50,51]. We aimed to investigate if calcium binding and therefore a potential membrane localization of VILIP-1 modulate the dimer formation. We found that in the presence of ionomycin, which increases intracellular calcium concentrations, oxidative VILIP-1 dimerization was enhanced in a dose-dependent manner (Fig. 5A). In contrast, lowering the intracellular calcium concentration with the membrane-permeative calcium chelator BAPTA resulted in a reduced dimer formation under oxidative conditions (Fig. 5B). It is of note that the administration of ionomycin or BAPTA without the oxidative challenge did not modify VILIP-1 dimerization (Figs. 5A and B). These data suggest that calcium binding and the subsequent reorganization of the protein structure facilitate dimer formation.

As calcium-bound VILIP-1 attaches to cellular membranes via its N-terminal myristoyl residue, we wondered whether calcium-dependent membrane localization is critical for dimerization. To test this hypothesis, we generated a myristoyl-deficient VILIP-1 mutant by changing Gly2 to an alanine (VILIP-1^{G2A}). Interestingly, VILIP-1^{G2A} dimerized upon H_2O_2 treatment to an even higher extent than VILIP-1^{WT} (Fig. 6A) and ionomycin treatment further enhanced this dimer formation (Fig. 6B). Moreover, also in cells transfected with VILIP-1^{G2A}, dimerization was suppressed after a preincubation with BAPTA before oxidative stimulation (Fig. 6C). This leads to the conclusion that dimerization of VILIP-1 depends on calcium inducing major conformational changes in the protein structure, but does not require the protein to be attached to cellular membranes with its myristoyl residue.

To track the subcellular localization of VILIP-1^{WT}, VILIP-1^{G2A}, and VILIP-1^{C187A}, we visualized VILIP-1 in transfected cells after treatment with either vehicle or H_2O_2 using immunofluorescence (Fig. 6D). Immunolabeling of VILIP-1 was specific, as we did not detect any signal in empty-vector-transfected cells. We observed a granular expression pattern for VILIP-1^{WT} in the cytoplasm as well as localization at the plasma membrane under control conditions. Interestingly, the same pattern, namely a localization at the plasma membrane, was also present in cells expressing VILIP-1^{C187A} and myristoyl-deficient VILIP-1^{G2A}. This shows that in our system, a certain amount of VILIP-1 localizes to the plasma membrane even in the absence of the myristoyl residue. Treatment with H_2O_2 did not change the subcellular localization of VILIP-1 notably.

Cys187-dependent VILIP-1 dimerization is a determinant of peroxide cytotoxicity

To investigate whether the dimerization of VILIP-1 plays a functional role in an oxidative environment, we exposed cells

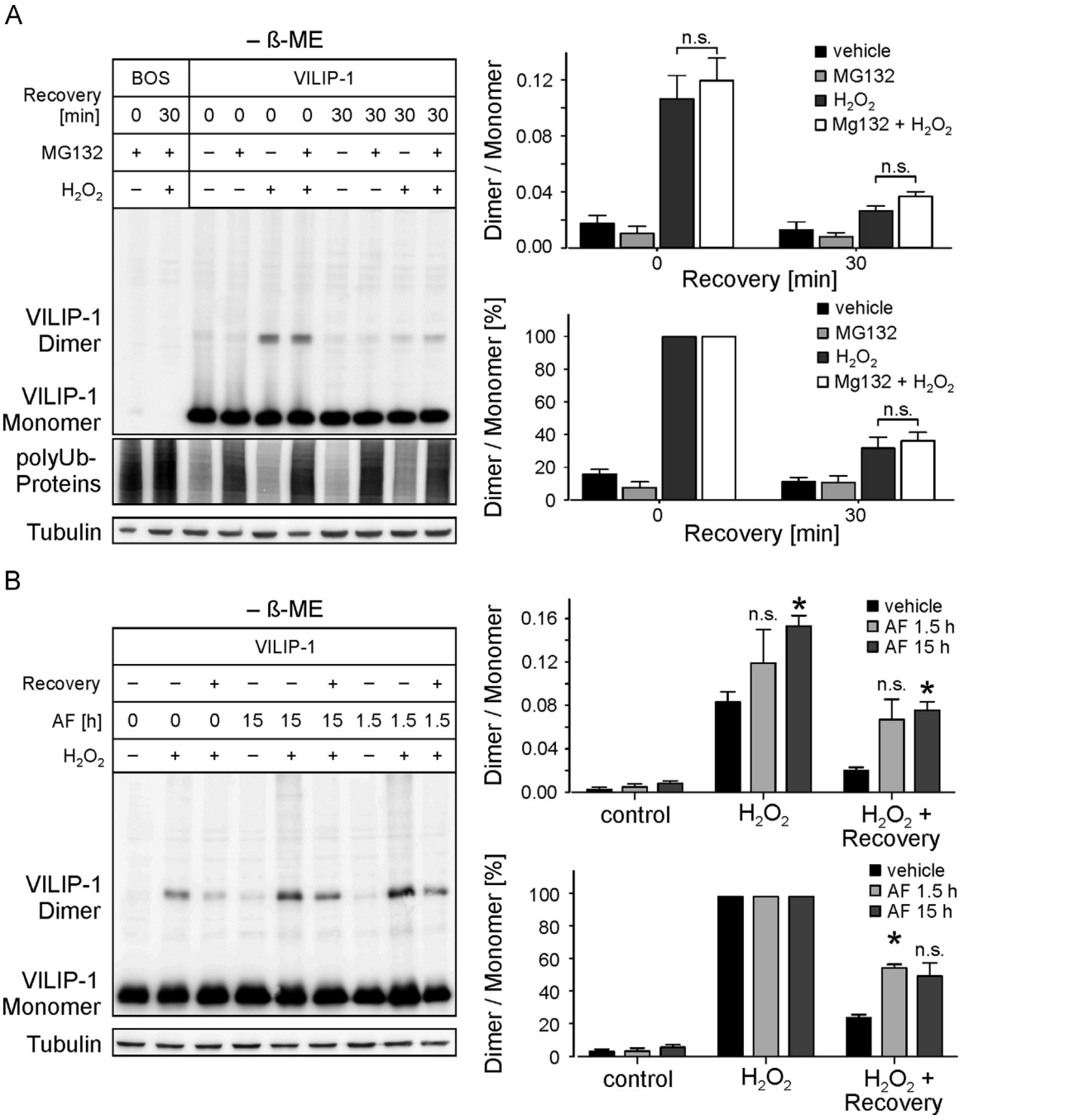

Fig. 3. The role of the thioredoxin system in the remonomerization of VILIP-1 dimers. (A and B) Total cell lysates (15 μg protein) were separated under nonreducing (−β-ME) and reducing (not shown) conditions on 12% SDS–polyacrylamide gels and analyzed by Western blotting. The ratios of VILIP-1 dimer vs monomer were calculated to normalize for transfection efficiency. The VILIP-1 dimer/monomer ratio after H_2O_2 treatment for 2 min without recovery was set to 100%. The mean values of (A) four and (B) three independent experiments ± SEM are shown. (A) VILIP-1^{WT}-transfected HEK293A cells were preincubated with either 20 μM MG-132 or vehicle for 20 min before adding 10 mM H_2O_2 for 2 min. Subsequently, the cells were either harvested or supplemented with fresh medium without H_2O_2 to recover in the presence or absence of 20 μM MG-132 for 30 min. Preincubation with MG-132 altered neither VILIP-1 dimerization in response to H_2O_2 (upper graph) nor the extend of recovery (lower graph). (B) VILIP-1^{WT}-transfected HEK293A cells were pretreated with 2 μM auranofin (AF) or vehicle for either 90 min or 15 h before addition of 10 mM H_2O_2 for 2 min. Subsequently, cells were either harvested or supplemented with fresh medium without H_2O_2 to recover in the presence or absence of 2 μM AF for 30 min. Preincubation with AF increased VILIP-1 dimerization in response to H_2O_2 compared to the vehicle-treated cells (upper graph). Recovery was impaired in cells preincubated with AF (for 15 h, $p=0.083$) (lower graph). $^*p < 0.05$.

transfected with VILIP-1^{WT}, VILIP-1^{G2A}, VILIP-1^{C187A}, or empty vector to a variety of physiologically relevant H_2O_2 concentrations for 18 h. We found that VILIP-1^{WT} overexpression significantly impaired the resistance of the cells to H_2O_2 compared to cells transfected with empty-vector control. The same was observed when the myristoyl-deficient mutant VILIP-1^{G2A} was expressed, implying that the role of VILIP-1 in enhancing H_2O_2 sensitivity is independent of its myristoyl residue. In contrast to this, no increased H_2O_2 sensitivity was measured when cells were transfected with VILIP-1^{C187A}, lacking the residue critical for dimerization (Fig. 7). Transfection efficiency was comparable between transfections with different VILIP-1 constructs (not shown), ruling out that the observed effect depended on different expression levels. These findings demonstrate that dimerization of VILIP-1 in response to oxidative stress might be involved in modulating cellular viability and cell death.

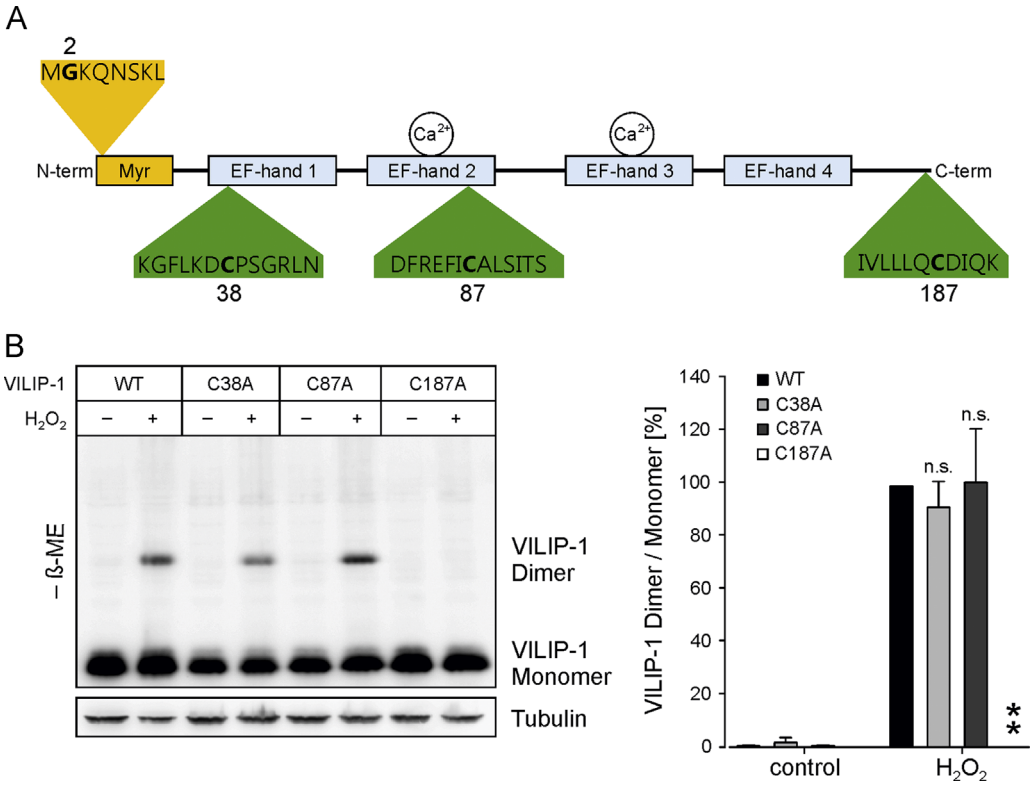

Fig. 4. VILIP-1 dimerization is mediated by Cys187. (A) Schematic representation of the primary protein structure of VILIP-1, highlighting the positions of the three cysteine residues and the N-terminal glycine, which is part of the conserved myristoylation sequence. (B) HEK293A cells were transfected with VILIP-1^{WT}, VILIP-1^{C38A}, VILIP-1^{C87A}, or VILIP-1^{C187A}. The cells were treated with either 10 mM H_2O_2 or vehicle for 10 min. 15 μg of total protein was separated under nonreducing (−β-ME) and reducing (not shown) conditions on 12% SDS–polyacrylamide gels and transferred to nitrocellulose membranes. To normalize for transfection efficiency, the VILIP-1 dimer/monomer ratio was calculated and set to 100% in the case of VILIP-1^{WT}. The mean value of three independent experiments ± SEM is shown. Dimerization of VILIP-1^{C38A} and VILIP-1^{C87A} due to oxidative treatment did not differ with respect to VILIP-1^{WT}. No dimer formation occurred between VILIP-1^{C187A} proteins. $^{**}p < 0.01$.

VILIP-1 is dimerized in animal models of ALS

After noting that VILIP-1 displays several features of a redox sensor in a cellular system, we were interested in whether dimerization of VILIP-1 plays a role in vivo in animal models of ALS. The presence of VILIP-1 dimers was investigated in extracts of spinal cord and cerebellum after tissue fractionation of total lysates, resulting in a soluble and an insoluble fraction enriched in SDS-resistant protein aggregates. We first analyzed the total lysate and the soluble fraction, containing proteins of potential functional relevance, in the presence and absence of reducing agent for the occurrence of VILIP-1 dimers. In nontransgenic and hSOD1^{WT}-overexpressing mice, not developing an ALS pathology, VILIP-1 dimers were hardly detectable in both fractions. In contrast, we found a significant increase in VILIP-1 dimers already at the onset of disease in spinal cords of mice expressing the ALS-causing hSOD1^{G93A} or hSOD1^{G85R} mutant. Dimer formation in spinal cord was also detected at disease end stage, but not in cerebellum of affected animals (Figs. 8A–D). In presymptomatic hSOD1^{mutant} mice, VILIP-1 dimer levels were not elevated compared to controls (Supplementary Fig. 3A). Prominent VILIP-1 dimer formation was also observed in the lumbar spinal cord of rats expressing hSOD1^{G93A}, but not in control animals (Supplementary Fig. 4A). In both animal models, no VILIP-1 dimers were detectable under reducing conditions, showing that the dimer was formed owing to an intermolecular disulfide bond like in HEK293A cells. Hence we have observed elevated steady-state levels of the dimers in a tissue-specific and disease-stage-dependent manner in animal models of ALS, a neurodegenerative disease characterized by increased levels of oxidative stress and elevated intracellular calcium.

VILIP-1 is enriched in ALS-specific protein aggregates

ALS is characterized by the formation of intracellular protein aggregates. As we found VILIP-1 disulfide-linked dimers early during the disease course, we aimed to investigate whether VILIP-1 is also part of ALS-specific aggregates. Therefore, we analyzed the aggregate-enriched fraction of the lumbar spinal cord and the cerebellum of hSOD1^{G93A} and hSOD1^{G85R} mice and age-matched controls. We used increasing amounts of detergents to enrich detergent-insoluble proteins via centrifugation steps to yield a fraction that remained insoluble in the presence of 0.5% NP-40, 0.5% desoxycholate, and 0.25% SDS [47]. We calculated the ratio of total protein in the aggregate-enriched fraction to total protein in the soluble fraction, resulting in increased ratios exclusively in the spinal cord, and not cerebellum, fraction of hSOD1^{mutant} mice at disease onset and disease end stage, showing that this method is suitable for enriching proteins that aggregate disease-dependently (Supplementary Fig. 2). Western blot analysis of the aggregate-enriched fraction under reducing conditions revealed VILIP-1 to be significantly enriched in the spinal cord of both hSOD1^{mutant} mouse strains (Fig. 9A). VILIP-1 was present in the aggregate-enriched fraction already at the onset of the disease. Interestingly, under nonreducing conditions, we observed that the additional amount of VILIP-1 in the aggregate-enriched fraction of hSOD1^{mutant} mice at disease end stage (and onset, not shown) refers to high-molecular-mass species > 190 kDa (Fig. 9B, top). As this smear was visible only under nonreducing conditions, VILIP-1 in this fraction seems to be aberrantly crosslinked via disulfide bonds with itself and/or other proteins (Fig. 9B, bottom). No aggregation of VILIP-1 was observed in the cerebellum of the same mice (Fig. 9A). Furthermore, in presymptomatic mice, in

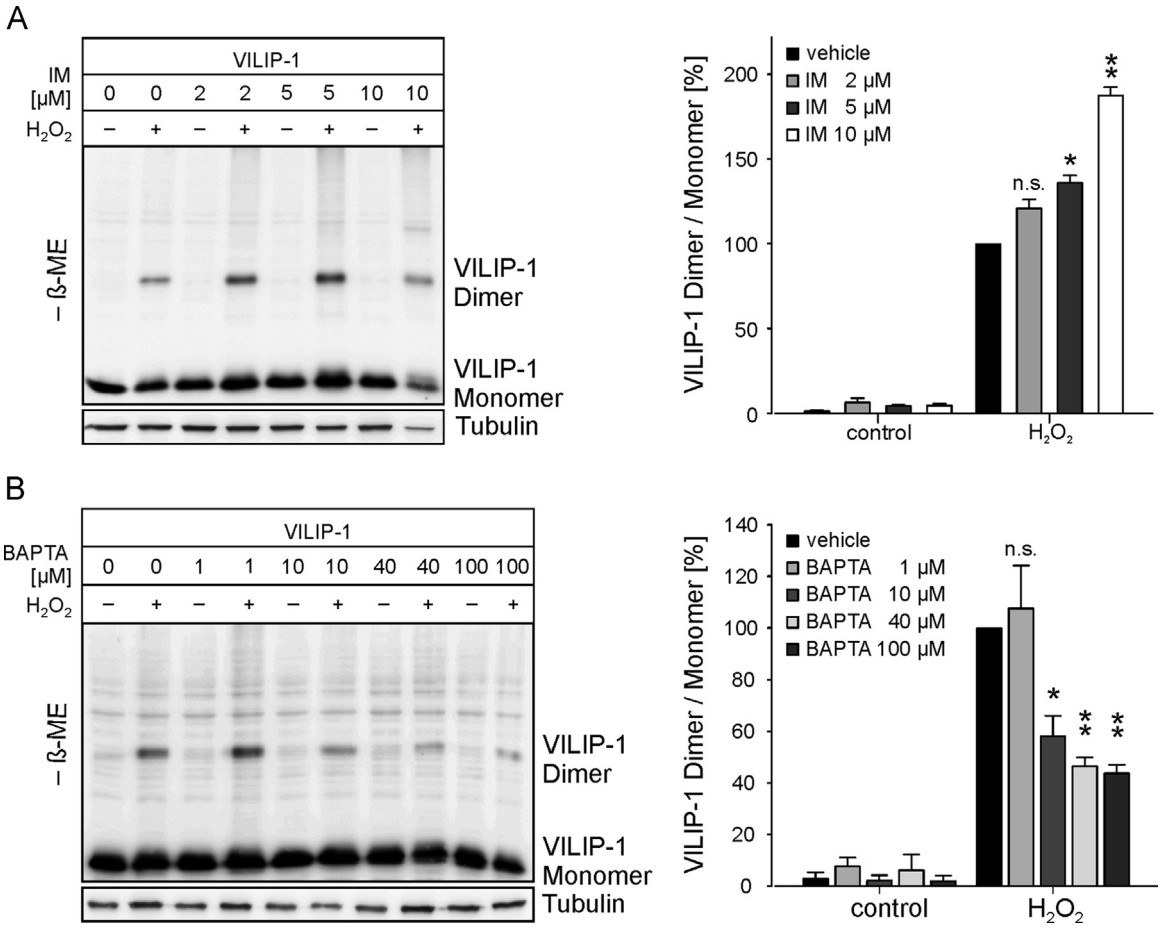

Fig. 5. Modulation of VILIP-1 dimerization by calcium. (A and B) HEK293A cells transfected with VILIP-1^{WT} were treated with 10 mM H_2O_2 for 10 min after a preincubation with (A) the indicated ionomycin (IM) concentrations for 5 min, or (B) the indicated BAPTA concentrations for 35 min, or vehicle for the appropriate time intervals. 15 μg of total protein was separated on nonreducing (−β-ME) and reducing (not shown) 12% SDS–polyacrylamide gels and analyzed by Western blotting. The ratios of VILIP-1 dimer to monomer were calculated to normalize for transfection efficiency. The VILIP-1 ratio from vehicle cells treated with H_2O_2 was set as 100%. The mean value ± SEM is shown for (A) three and (B) four independent experiments. Statistical analysis was performed within the H_2O_2-treated group between vehicle-treated cells and IM- or BAPTA-treated cells. (A) The VILIP-1 dimer-to-monomer ratio was increased dependent on IM treatment. This was significant according to treatment with 5 or 10 μM IM. (B) Preincubation with 10, 40, or 100 μM BAPTA significantly reduced the VILIP-1 dimer/monomer ratio. $^{*}p < 0.05$, $^{**}p < 0.01$.

which we also failed to detect hSOD1^{mutant} in the aggregate-enriched fraction, no aggregation of VILIP-1 was detected, indicating that VILIP-1 and hSOD1^{mutant} aggregate approximately at the same time (Supplementary Fig. 3B). Moreover, we investigated the aggregate-enriched fractions of spinal cords of hSOD1^{WT} and hSOD1^{G93A} rats at the end stage of the disease. Also here, we found VILIP-1 to aggregate ALS-specifically, showing that entrapment of VILIP-1 in aggregates is not restricted to mouse models of the disease (Supplementary Fig. 4B).

In a second approach, aiming to get deeper insight into the composition of the protein aggregates in ALS mouse models, we performed label-free LC–MSE mass spectrometry of insoluble spinal cord fractions from hSOD1^{mutant} mice at the end stage of the disease and from age-matched controls. The quantitative analysis revealed hSOD1^{mutant} itself as well as ubiquitin to be enriched in the insoluble fractions of both mouse models of ALS. In addition to these proteins serving as positive controls, we found VILIP-1 to be significantly enriched in an ALS-specific manner (Table 1).

To summarize these findings, VILIP-1 is prone to redox-dependent crosslinking in two different animal models of ALS specifically in the affected tissue beginning with the onset of the disease. The observed aggregation pattern of VILIP-1 is comparable with the aggregation pattern of hSOD1^{mutant}.

Discussion

Specificity of VILIP-1 dimer formation and remonomerization

We have shown for the first time in an intact cellular environment that disulfide-linked VILIP-1 homodimers form upon stimulation with oxidants such as H_2O_2 or diamide in a time- and concentration-dependent manner. This is in line with earlier findings showing that VILIP-1 is able to dimerize via disulfide bonds in vitro depending on the oxidative status [12,13]. We demonstrate that Cys187 at the flexible C-terminus exclusively mediates disulfide bond formation in vivo, whereas Cys38 and Cys87 do not contribute to dimerization. This is partly supported by in vitro data showing that a mutation of Cys187 reduced, but not completely prevented, dimer formation, indicating that in that system also Cys38 and Cys87 were involved in disulfide bond formation [12]. In this context it is remarkable that in the three-dimensional structure of VILIP-1, Cys38 was shown to sit at the rim of a hydrophobic cleft, being at least partially exposed [10]. The lack of participation of Cys38 in dimer formation in vivo highlights the specificity of the Cys187 interaction, as in the case of random disulfide crosslinking, Cys38 should also be involved in dimer formation. The specificity of VILIP-1 dimerization is strongly supported by the formation of a distinct VILIP-1 dimer band after

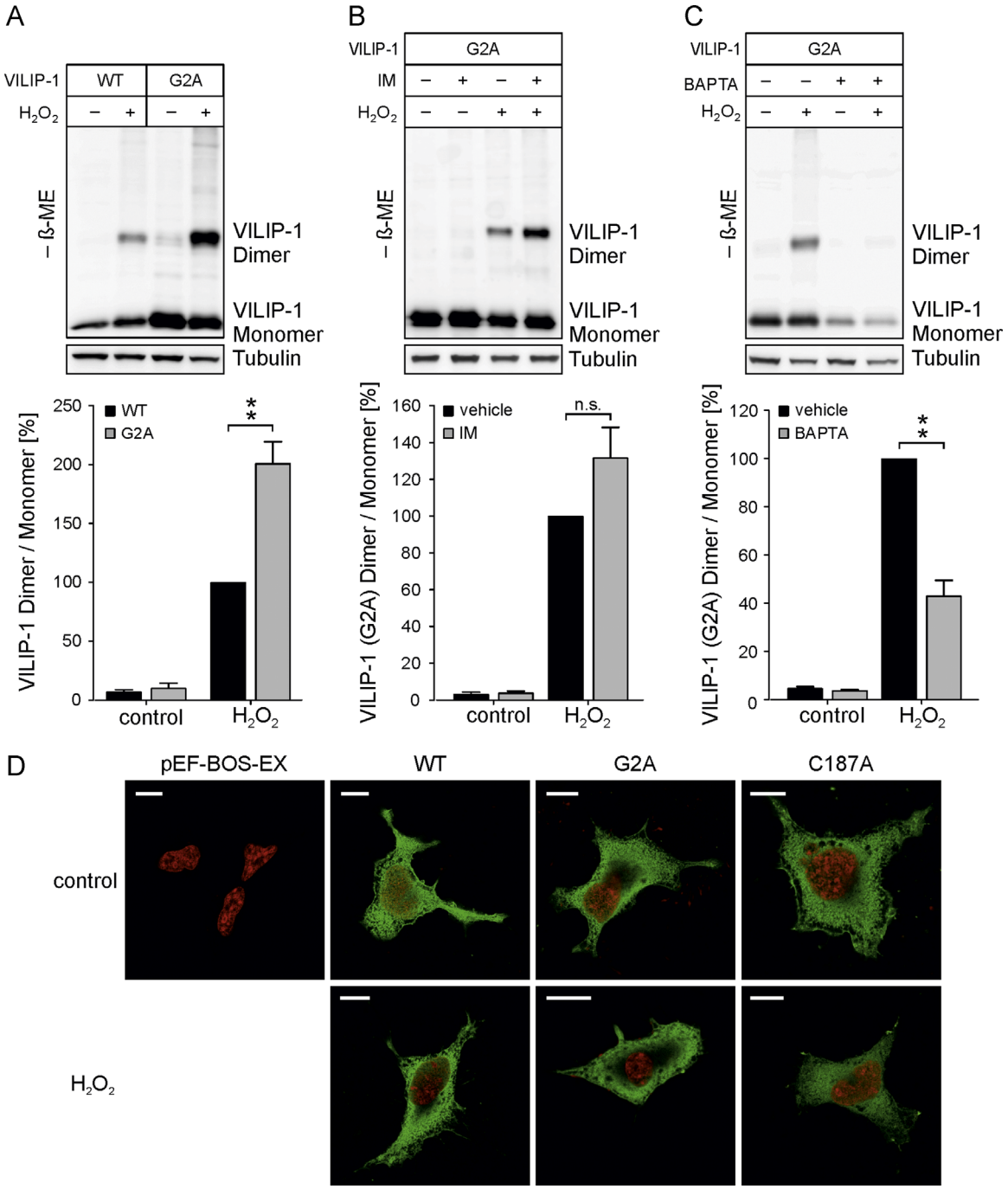

Fig. 6. VILIP-1 dimerization of a myristoyl-deficient VILIP-1 mutant. (A–C) HEK293A cells transfected with (A) VILIP-1^{WT} or (A–C) VILIP-1^{G2A} were treated with 10 mM H_2O_2 for 10 min (A) without or with preincubation of (B) 5 μM ionomycin (IM) for 5 min or (C) 40 μM BAPTA for 35 min, or appropriate vehicle. 15 μg of total protein lysates was separated under nonreducing (−β-ME) or reducing (not shown) conditions on 12% SDS–polyacrylamide gels and analyzed by Western blotting. The ratios of VILIP-1 monomer to dimer were calculated and data were normalized to control conditions (10 mM H_2O_2 for 10 min). Densitometric analysis ± SEM of (A) five, (B) four, and (C) four independent experiments is shown. (A) Dimerization of VILIP-1^{G2A} in response to H_2O_2 was significantly greater than dimerization of VILIP-1^{WT}. (B) A trend to increased dimerization of VILIP-1^{G2A} preincubated with IM was observed. (C) H_2O_2-dependent dimerization of VILIP-1^{G2A} was significantly reduced according to preincubation with BAPTA. (D) HEK293A cells were transfected with VILIP-1^{WT}, VILIP-1^{G2A}, VILIP-1^{C187A}, or the empty pEF-BOS-EX vector. Cells were treated with either 10 mM H_2O_2 or vehicle for 10 min. For immunolabeling, Cy2-coupled secondary antibody was used to label VILIP-1, which is shown in green. DAPI staining is shown in red. $^{**}p < 0.01$.

oxidative challenge, rather than the appearance of a smear in the Western blot analysis.

All five NCS class B proteins (VILIP-1 to -3, hippocalcin, neurocalcin δ), but no other members of the NCS protein family, possess the Cys187 residue. Therefore, Cys187-mediated dimerization could be relevant in all NCS class B proteins. Earlier, the NCS class C protein recoverin was proposed to be redox sensitive, dimerizing via an intermolecular disulfide bond with the highly conserved Cys38 residue under conditions of oxidative stress in vitro [52]. This dimerization was reversible and modulated by calcium. In contrast to recoverin, Cys38 was not involved in dimerization of VILIP-1. Moreover, a whole range of NCS proteins, including guanylyl-cyclase activating protein-2, neurocalcin δ, and calsenilin (also known as DREAM or KChIP3), undergo functional dimerization, although in these cases dimerization was mediated by noncovalent interactions [53–55]. Recently, noncovalent dimerization has also been proposed for VILIP-1 [11,13]. We suggest that noncovalently linked dimers of VILIP-1 might act as precursors for the specific

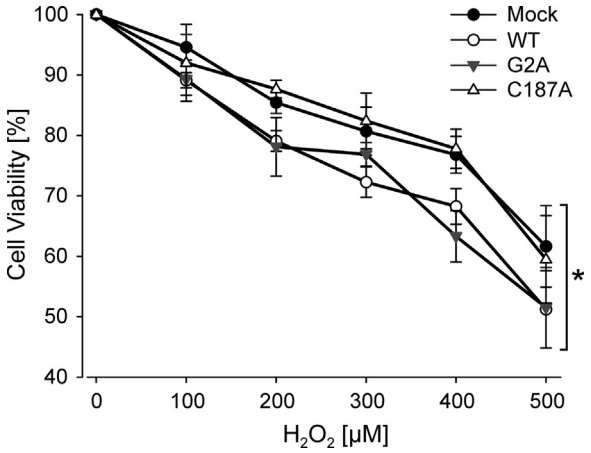

Fig. 7. Impact of VILIP-1 dimerization on H_2O_2 sensitivity. 5000 HEK293A cells transfected with VILIP-1^{WT}, VILIP-1^{C187A}, VILIP-1^{G2A}, or empty vector per well were treated with the indicated concentrations of H_2O_2 for 18 h before addition of MTT for 3 h. For each transfection the mean absorption of six vehicle-treated wells was normalized to 100%. The percentage of the mean absorption measured for each H_2O_2 concentration compared to the mean absorption of vehicle-treated cells was calculated. Cell viability was plotted against concentrations of H_2O_2. Shown is the mean value of cell viability ± SEM of four or more independently performed experiments. Survival of cells upon treatment with H_2O_2 was significantly impaired in cells transfected with VILIP-1^{WT} and VILIP-1^{G2A} compared to both mock- and VILIP-1^{C187A}-transfected cells. Transfection efficiency between cells transfected with different VILIP-1 constructs was comparable (not shown). *$p < 0.05$.

disulfide-linked dimerization after an oxidative stimulus. A similar mechanism was found to regulate the activity of ataxia-telangiectasia mutated protein kinase in response to oxidative stress, where only the disulfide-linked dimer was functionally active [56]. Although only a relatively small proportion of VILIP-1 formed dimers, they should be sufficient to affect cellular fate if involved in a signal transduction cascade. In this context it is noteworthy that VILIP-1 has been shown to increase cellular cGMP levels by acting on guanylyl-cyclase B [14,17], and conditions leading to dimerization of VILIP-1 were accompanied by elevated cGMP generation in vitro [12].

As a role for VILIP-1 dimers in the regulation of protein function and cellular signaling demands a mechanism to remove the dimers efficiently at the end of oxidative stimulation, we investigated the thioredoxin system, which we found to be involved in the remonomerization of VILIP-1. The thioredoxin system is an important component of the antioxidative defense and involved in the redox regulation of the cellular stress response [57]. As a putative part of the so-called vitagene network [58,59], thioredoxins are a critical component to balance the redox equilibrium, thereby promoting longevity [60,61]. This regulation may be impaired by the chronic oxidative burden found in many neurodegenerative diseases that results in an imbalance of various cellular systems such as the proteostasis network [62]. In addition, thioredoxins are directly involved in redox signaling upon acute oxidative stress by reducing and thus inactivating transcription factors such as Yap1, which is activated by H_2O_2-mediated intramolecular disulfide bond formation [2]. The rapid dimer formation of VILIP-1 under conditions of oxidative stress as well as the efficient remonomerization promptly after shifting the oxidative environment toward reducing conditions meets the criteria for redox sensors and makes the dimer a potential candidate executing a distinct cellular function in response to oxidative stress.

The role of calcium and the myristoyl residue in VILIP-1 dimer formation

Disulfide bond-mediated dimerization of recoverin and VILIP-1 in vitro has been shown to strongly depend on calcium [12,52]. Therefore we investigated the role of calcium on dimer formation of VILIP-1 in an intact cellular system. Myristoylated VILIP-1 has been shown to bind two calcium ions under physiological conditions [10]. Nonmyristoylated VILIP-1 binds calcium with higher affinity than the myristoylated protein, whereas the positive cooperativity between the EF-hands is reduced [11], a phenomenon also evident in recoverin and neurocalcin δ [63,64]. We found that calcium triggers redox-induced dimerization of VILIP-1 independent of protein myristoylation. This finding contradicted our initial hypothesis that only the pool of calcium-bound VILIP-1 proteins attached to membranes via their myristoyl residues should be sensitive to oxidant-induced dimerization. In fact, a myristoyl-deficient VILIP-1 mutant (VILIP-1^{G2A}) dimerized to an even higher extent than VILIP-1^{WT}, and increased intracellular calcium concentrations further enhanced the dimerization of VILIP-1^{G2A}. This could be explained by the increased affinity of nonmyristoylated VILIP-1 for calcium [11].

It has been shown that calcium binding to NCS induces major conformational rearrangements beyond the extrusion of the myristoyl residue, exposing a variety of hydrophobic residues [6,8,11,65]. We propose that these structural changes make the C-terminus of VILIP-1 more prone to dimerization. In this context it would be possible that calcium-dependent VILIP-1 dimerization in the cytoplasm is crucial for the subsequent relocalization of VILIP-1 to cellular membranes. More recent studies, however, discuss the role of the myristoyl residue in anchoring VILIP-1 to cellular membranes more controversially and propose a model in which the protein, also in the calcium-free state, is attached to membranes via hydrophobic interactions independent of myristoylation [13]. In this model the myristoyl residue, after calcium binding, serves either in enhancing membrane association or in interacting with target proteins. This hypothesis is supported by findings that recoverin associates with hydrophobic structures upon calcium binding independent of its myristoylation [6] and by a study in PC12 cells, in which nonmyristoylated VILIP-1 also revealed a weak membrane association [50]. This concept is supported by our data, in that a weak membrane staining was observed for VILIP-1^{WT}, VILIP-1^{G2A}, and VILIP-1^{C187A} also in the absence of calcium. In line with this, it is possible that a pool of membrane-associated VILIP-1 is particularly prone to dimerization upon an oxidative stimulus, potentially because of the close proximity of several VILIP-1 proteins at distinct membrane loci.

The role of Cys187 in modulating sensitivity of cells to oxidative stress

We found that transgenic expression of VILIP-1 in HEK293A cells significantly enhances sensitivity to physiologically relevant concentrations of H_2O_2 upon long-term exposure. This property of VILIP-1 was independent of its myristoylation. Interestingly, in contrast to VILIP-1^{WT} and VILIP-1^{G2A}, VILIP-1 lacking the Cys187 residue critical for dimerization did not impair cell survival in response to H_2O_2. From these findings, we conclude that dimerization of VILIP-1 plays a critical role in the modulation of survival upon long-term oxidative stress. The effect of VILIP-1 on cellular survival has so far been investigated only under conditions of calcium stress. Results from these studies are contradictory, as VILIP-1 either protected from or enhanced calcium-induced cell death in adrenocortical carcinoma cells or PC12 cells, respectively [27,66]. Furthermore, hippocalcin, another NCS class B subfamily member with 68% protein sequence identity to VILIP-1, protected neuronal cell lines from calcium-induced apoptosis. The antiapoptotic effect was mediated by the interaction with the neuronal apoptosis inhibitory protein, which has been linked to the degeneration of motor neurons in spinal muscular atrophy [67–69]. Further studies are necessary to investigate the function of VILIP-1

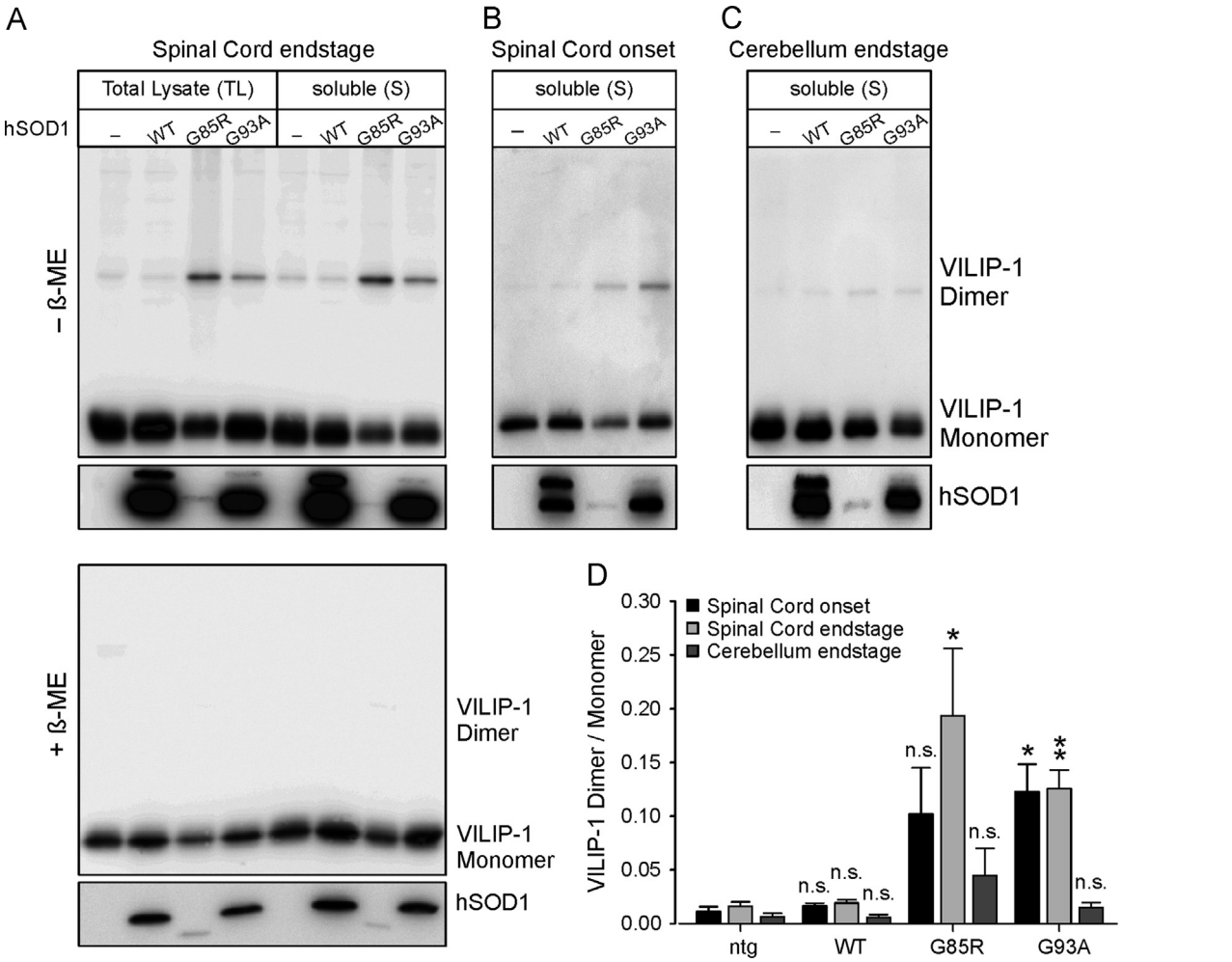

Fig. 8. VILIP-1 dimerization in mouse models of ALS. (A–D) Lumbar spinal cord and cerebellum of nontransgenic mice and mice overexpressing hSOD1^{WT}, hSOD1^{G93A}, or hSOD1^{G85R} at onset or end stage of the disease were fractionated, yielding a total lysate, a soluble fraction, and an aggregate-enriched fraction. Shown is the medium value ± SEM of (A) five (spinal cord end stage), (B) three (spinal cord onset), or (C) three (cerebellum end stage) independent tissue fractionations of different mice. The total lysate and the soluble fraction (both 5 μg) were separated on 15% SDS–polyacrylamide gels under nonreducing (−β-ME) or reducing (+β-ME; lower blot in (A); not shown for (B) and (C)) conditions and transferred to nitrocellulose membranes. (D) To normalize for total expression level of VILIP-1, the band intensity of the VILIP-1 dimer was divided by the band intensity of the VILIP-1 monomer. The VILIP-1 dimer/monomer ratio was significantly greater in the spinal cords of SOD1^{mutant} mice at disease onset (SOD1^{G93A}) as well as at disease end stage (SOD1^{G93A}, SOD1^{G85R}), but not in the cerebella of mice at disease end stage. *$p < 0.05$, **$p < 0.01$.

dimerization in mediating the increased oxidative sensitivity of cells upon VILIP-1 overexpression.

Dimerization and aggregation of VILIP-1 in ALS

ALS is a neurodegenerative disease that is characterized by increased levels of oxidative stress and excitotoxicity that mutually enhance each other [31]. We found that VILIP-1 dimers are present in the spinal cord of mutant SOD1 animals from disease onset onward. The observation that VILIP-1 dimerization makes cells more sensitive to oxidative insults might provide a direct link between oxidative stress, increased calcium levels, and the loss of motor neurons. Furthermore, concomitant with disease onset, VILIP-1 has been detected in protein aggregates. Although it is tempting to assume that dimer formation by Cys187 is simply a prerequisite of aggregate formation, our data suggest that both processes could contribute to disease progression independently.

The investigation of VILIP-1 as a redox sensor and as a possible mediator of toxicity in ALS is of particular interest as there is a growing body of literature indicating that sensing the oxidative status of the cell is a key event for the regulation of vitagenes that include molecular chaperones and antioxidative enzymes such as thioredoxins [70]. Nevertheless, the capacity for a continuous adaptation to chronic oxidative stress is limited, particularly in neurons affected by neurodegenerative diseases, and might therefore result in VILIP-1 dimerization. A specific role for VILIP dimers for cell survival is supported by the observation that cysteine-linked VILIP-1 dimers were detected only in affected tissues of diseased animals, suggesting that in healthy control mice dimer formation is strictly regulated. This is in line with our data showing that VILIP-1 dimerization is completely reversible after a short oxidative insult, indicating a functional relevance for VILIP-1 dimer formation in redox signaling. In contrast, increasing oxidative burden and elevated calcium levels over a long period of time, as observed in ALS [31], might overwhelm the cellular antioxidant defense systems. As a consequence, dimerized VILIP-1 accumulates and thus damages the cell. Recently, a similar mechanism has been proposed for the transactivation response DNA-binding protein of 43 kDa (TDP-43), a major disease protein in ALS. TDP-43 is involved in redox signaling via cysteine oxidation and subsequent relocation from the nucleus to the cytosol [71], implying that cysteine oxidation is an upstream event in TDP-43 toxicity and that redox signaling is of broader relevance in ALS.

High-molecular-weight protein species detected in the aggregate-enriched fraction by VILIP-1 antibodies suggest a rather unorganized accumulation of proteins and are in contrast to the

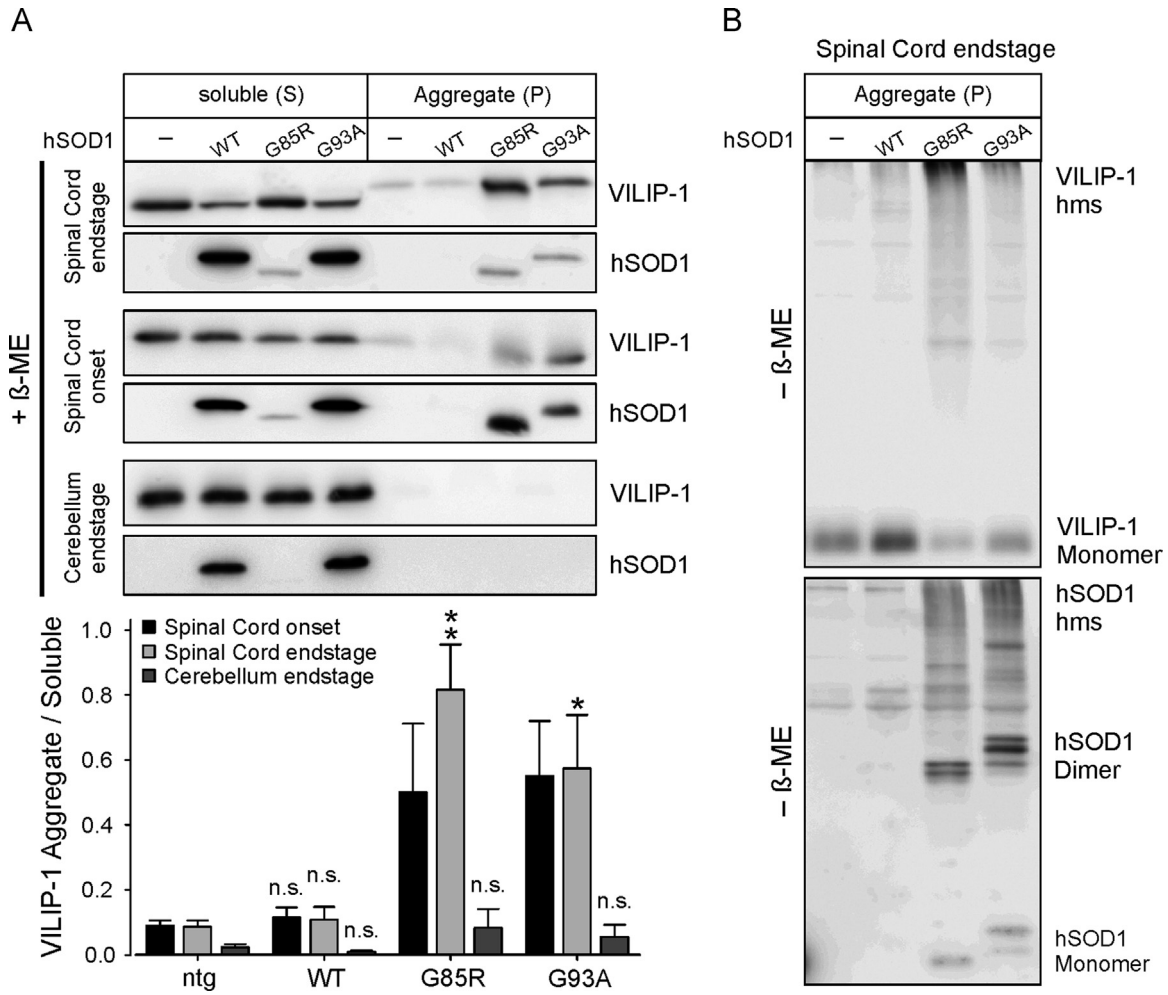

Fig. 9. VILIP-1 aggregation in mouse models of ALS. (A) Extracts from the same fractionation as described for Fig. 7 were analyzed. The soluble fraction and the aggregate-enriched fraction (5 μg each) were separated on 15% SDS–polyacrylamide gels under reducing (−β-ME) conditions and analyzed by Western blotting. VILIP-1 and hSOD1 were enriched in the aggregate-enriched fraction of spinal cords of $SOD1^{mutant}$ mice at onset and end stage of the disease (significantly at disease end stage), but not in the cerebella of mice at disease end stage. Statistical analysis was performed for each tissue compared to nontransgenic littermates. (B) The aggregate-enriched fraction (5 μg) of spinal cords at disease end stage shown in (A) were separated on 15% SDS–polyacrylamide gels under nonreducing conditions. ALS-specifically enriched VILIP-1 in the aggregate-enriched fraction is present as a high-molecular-mass species (hms) due to disulfide crosslinking (top). $hSOD1^{mutant}$ in the aggregate-enriched fraction under nonreducing conditions is present as aberrantly linked dimeric and multimeric species (bottom). $^{*}p < 0.05$, $^{**}p < 0.01$.

Table 1
VILIP-1 was revealed to be enriched in label-free LC–MSE mass spectrometric analysis of ALS aggregates.

Genotype	G93A/ntg (*x*-fold)	G93A/WT (*x*-fold)	G85R/ntg (*x*-fold)	G85R/WT (*x*-fold)
SOD1	23.37	9.76	19.53	8.15
Ubiquitin	2.56	2.39	2.26	2.11
VILIP-1	2.35	2.09	2.94	2.60

Insoluble fractions of control mice (ntg, $SOD1^{WT}$) and $SOD1^{G93A}$ and $SOD1^{G85R}$ mice at disease end stage were analyzed by label-free mass spectrometric analysis. VILIP-1 was enriched in the insoluble fractions of both $SOD1^{mutant}$ mouse strains compared to both ntg and $SOD1^{WT}$ mice. SOD1 and ubiquitin functioned as positive controls. ntg, nontransgenic.

very specific Cys187-mediated dimerization of VILIP-1 described above. VILIP-1 oligomerization is induced upon calcium binding in vitro and in vivo [11,72]. We propose that VILIP-1 interacts with hydrophobic surfaces on protein aggregates by exposing the myristoyl residue upon elevated calcium levels in the course of disease. In a second step, aberrant disulfide crosslinking occurs between proteins in close proximity. Such a two-step process has also been described for mutant SOD1 aggregate formation [73]. As a result, functional VILIP-1 levels are reduced and might thus contribute to disease by a loss of function. In this context it is noteworthy that whole genome expression profiling revealed VILIP-1 mRNA to be downregulated in the motor cortex of sporadic ALS patients [29].

In addition to ALS, VILIP-1 expression is reduced in AD patients at the protein as well as the transcription level [26,74]. In addition, VILIP-1 has been shown to be associated with amyloid plaques and tangles [27]. In contrast, VILIP-1 levels are increased in the cerebrospinal fluid of AD patients and were suggested as an early biomarker for cognitive decline [75–77]. With respect to our findings that VILIP-1 dimerizes and aggregates in ALS, VILIP-1 might play multiple roles in a broader range of neurodegenerative diseases.

Acknowledgments

We are very grateful to the following colleagues for providing reagents: Professor K.H. Braunewell (Southern Research Institute, Birmingham, AL, USA) for the $VILIP\text{-}1^{WT\text{-}GFP}$ plasmid, Professor S. Nagata (Department of Medical Chemistry, Kyoto University, Japan) for the pEF-BOS-EX vector, Professor D. Cleveland (University of California at San Diego, La Jolla, CA, USA) for $SOD1^{G85R}$

mice, and Dr. S. Boillee and Dr. C. Lobsiger (ICM Brain and Spine Institute, Paris, France) for tissues from transgenic rats. We thank Dr. H. Witan and S. Fritschi for initial experiments and Dr. I. Zwiener (IMBEI, University Medical Center, Mainz, Germany) for competent counselling on statistical analysis. M.P.L. and A.M.K. were members of the Neuroscience Graduate School (DFG/GRK 1088). This work was supported in part by the German Foundation for Muscle Diseases (DGM e.V.; to A.M.C.), the Stiftung Rheinland Pfalz fuer Innovation (to A.M.C. and C.B.), and the Collaborative Research Center "Neuronal Homeostasis" (DFG/CRC 1080) (to A.M.C. and C.B.). S.T. was supported by the Forschungszentrum Immunologie and the Naturwissenschaftlich-Medizinisches Forschungszentrum of the Johannes-Gutenberg University Mainz. A.M.C. and C.B. are members of the Focus Program Translational Neuroscience (University of Mainz) and part of the German Network for Motor Neuron diseases "MND-Net" (BMBF), as is Professor M. Sendtner (Neurology, University of Wuerzburg, Germany), who kindly provided $SOD1^{WT}$ and $SOD1^{G93A}$ mice.

Appendix A. Supplementary material

Supplementary data associated with this article can be found in the online version at http://dx.doi.org/10.1016/j.freeradbiomed.2014.04.008.

References

[1] Vazquez-Torres, A. Redox active thiol sensors of oxidative and nitrosative stress. *Antioxid. Redox Signaling* **17:**1201–1214; 2012.
[2] Delaunay, A.; Isnard, A. D.; Toledano, M. B. H_2O_2 sensing through oxidation of the Yap1 transcription factor. *EMBO J.* **19:**5157–5166; 2000.
[3] Cumming, R. C.; Andon, N. L.; Haynes, P. A.; Park, M.; Fischer, W. H.; Schubert, D. Protein disulfide bond formation in the cytoplasm during oxidative stress. *J. Biol. Chem.* **279:**21749–21758; 2004.
[4] Klomsiri, C.; Karplus, P. A.; Poole, L. B. Cysteine-based redox switches in enzymes. *Antioxid. Redox Signaling* **14:**1065–1077; 2011.
[5] Braunewell, K. H.; Gundelfinger, E. D. Intracellular neuronal calcium sensor proteins: a family of EF-hand calcium-binding proteins in search of a function. *Cell Tissue Res.* **295:**1–12; 1999.
[6] Zozulya, S.; Stryer, L. Calcium–myristoyl protein switch. *Proc. Natl. Acad. Sci. USA* **89:**11569–11573; 1992.
[7] Dizhoor, A. M.; Chen, C. K.; Olshevskaya, E.; Sinelnikova, V. V.; Phillipov, P.; Hurley, J. B. Role of the acylated amino terminus of recoverin in Ca^{2+}-dependent membrane interaction. *Science* **259:**829–832; 1993.
[8] Ames, J. B.; Ishima, R.; Tanaka, T.; Gordon, J. I.; Stryer, L.; Ikura, M. Molecular mechanics of calcium–myristoyl switches. *Nature* **389:**198–202; 1997.
[9] Burgoyne, R. D.; O'Callaghan, D. W.; Hasdemir, B.; Haynes, L. P.; Tepikin, A. V. Neuronal Ca^{2+}-sensor proteins: multitalented regulators of neuronal function. *Trends Neurosci.* **27:**203–209; 2004.
[10] Cox, J. A.; Durussel, I.; Comte, M.; Nef, S.; Nef, P.; Lenz, S. E.; Gundelfinger, E. D. Cation binding and conformational changes in VILIP and NCS-1, two neuron-specific calcium-binding proteins. *J. Biol. Chem.* **269:**32807–32813; 1994.
[11] Li, C.; Pan, W.; Braunewell, K. H.; Ames, J. B. Structural analysis of Mg^{2+} and Ca^{2+} binding, myristoylation, and dimerization of the neuronal calcium sensor and visinin-like protein 1 (VILIP-1). *J. Biol. Chem.* **286:**6354–6366; 2011.
[12] Chen, K. C.; Wang, L. K.; Chang, L. S. Regulatory elements and functional implication for the formation of dimeric visinin-like protein-1. *J. Pept. Sci.* **15:**89–94; 2009.
[13] Wang, C. K.; Simon, A.; Jessen, C. M.; Oliveira, C. L.; Mack, L.; Braunewell, K. H.; Ames, J. B.; Pedersen, J. S.; Hofmann, A. Divalent cations and redox conditions regulate the molecular structure and function of visinin-like protein-1. *PLoS One* **6:**e26793; 2011.
[14] Braunewell, K. H.; Brackmann, M.; Schaupp, M.; Spilker, C.; Anand, R.; Gundelfinger, E. D. Intracellular neuronal calcium sensor (NCS) protein VILIP-1 modulates cGMP signalling pathways in transfected neural cells and cerebellar granule neurones. *J. Neurochem.* **78:**1277–1286; 2001.
[15] Braunewell, K. H.; Spilker, C.; Behnisch, T.; Gundelfinger, E. D. The neuronal calcium-sensor protein VILIP modulates cyclic AMP accumulation in stably transfected C6 glioma cells: amino-terminal myristoylation determines functional activity. *J. Neurochem.* **68:**2129–2139; 1997.
[16] Lin, L.; Jeanclos, E. M.; Treuil, M.; Braunewell, K. H.; Gundelfinger, E. D.; Anand, R. The calcium sensor protein visinin-like protein-1 modulates the surface expression and agonist sensitivity of the alpha 4beta 2 nicotinic acetylcholine receptor. *J. Biol. Chem.* **277:**41872–41878; 2002.
[17] Brackmann, M.; Schuchmann, S.; Anand, R.; Braunewell, K. H. Neuronal Ca^{2+} sensor protein VILIP-1 affects cGMP signalling of guanylyl cyclase B by regulating clathrin-dependent receptor recycling in hippocampal neurons. *J. Cell Sci.* **118:**2495–2505; 2005.
[18] Dai, F. F.; Zhang, Y.; Kang, Y.; Wang, Q.; Gaisano, H. Y.; Braunewell, K. H.; Chan, C. B.; Wheeler, M. B. The neuronal Ca^{2+} sensor protein visinin-like protein-1 is expressed in pancreatic islets and regulates insulin secretion. *J. Biol. Chem.* **281:**21942–21953; 2006.
[19] Zhao, C.; Anand, R.; Braunewell, K. H. Nicotine-induced Ca^{2+}-myristoyl switch of neuronal Ca^{2+} sensor VILIP-1 in hippocampal neurons: a possible crosstalk mechanism for nicotinic receptors. *Cell. Mol. Neurobiol.* **29:**273–286; 2009.
[20] Zhao, C. J.; Noack, C.; Brackmann, M.; Gloveli, T.; Maelicke, A.; Heinemann, U.; Anand, R.; Braunewell, K. H. Neuronal Ca^{2+} sensor VILIP-1 leads to the upregulation of functional alpha4beta2 nicotinic acetylcholine receptors in hippocampal neurons. *Mol. Cell. Neurosci.* **40:**280–292; 2009.
[21] Mathisen, P. M.; Johnson, J. M.; Kawczak, J. A.; Tuohy, V. K. Visinin-like protein (VILIP) is a neuron-specific calcium-dependent double-stranded RNA-binding protein. *J. Biol. Chem.* **274:**31571–31576; 1999.
[22] Mahloogi, H.; Gonzalez-Guerrico, A. M.; Lopez De Cicco, R.; Bassi, D. E.; Goodrow, T.; Braunewell, K. H.; Klein-Szanto, A. J. Overexpression of the calcium sensor visinin-like protein-1 leads to a cAMP-mediated decrease of in vivo and in vitro growth and invasiveness of squamous cell carcinoma cells. *Cancer Res.* **63:**4997–5004; 2003.
[23] Fu, J.; Jin, F.; Zhang, J.; Fong, K.; Bassi, D. E.; Lopez De Cicco, R.; Ramaraju, D.; Braunewell, K. H.; Conti, C.; Benavides, F.; Klein-Szanto, A. J. VILIP-1 expression in vivo results in decreased mouse skin keratinocyte proliferation and tumor development. *PLoS One* **5:**e10196; 2010.
[24] Schonrath, K.; Pan, W.; Klein-Szanto, A. J.; Braunewell, K. H. Involvement of VILIP-1 (visinin-like protein) and opposite roles of cyclic AMP and GMP signaling in in vitro cell migration of murine skin squamous cell carcinoma. *Mol. Carcinog.* **50:**319–333; 2011.
[25] Braunewell, K. H.; Brackmann, M.; Manahan-Vaughan, D. Group I mGlu receptors regulate the expression of the neuronal calcium sensor protein VILIP-1 in vitro and in vivo: implications for mGlu receptor-dependent hippocampal plasticity? *Neuropharmacology* **44:**707–715; 2003.
[26] Braunewell, K.; Riederer, P.; Spilker, C.; Gundelfinger, E. D.; Bogerts, B.; Bernstein, H. G. Abnormal localization of two neuronal calcium sensor proteins, visinin-like proteins (vilips)-1 and -3, in neocortical brain areas of Alzheimer disease patients. *Dementia Geriatr. Cognit. Disord.* **12:**110–116; 2001.
[27] Schnurra, I.; Bernstein, H. G.; Riederer, P.; Braunewell, K. H. The neuronal calcium sensor protein VILIP-1 is associated with amyloid plaques and extracellular tangles in Alzheimer's disease and promotes cell death and tau phosphorylation in vitro: a link between calcium sensors and Alzheimer's disease? *Neurobiol. Dis.* **8:**900–909; 2001.
[28] Bernstein, H. G.; Becker, A.; Keilhoff, G.; Spilker, C.; Gorczyca, W. A.; Braunewell, K. H.; Grecksch, G. Brain region-specific changes in the expression of calcium sensor proteins after repeated applications of ketamine to rats. *Neurosci. Lett.* **339:**95–98; 2003.
[29] Lederer, C. W.; Torrisi, A.; Pantelidou, M.; Santama, N.; Cavallaro, S. Pathways and genes differentially expressed in the motor cortex of patients with sporadic amyotrophic lateral sclerosis. *BMC Genomics* **8:**26; 2007.
[30] Barber, S. C.; Mead, R. J.; Shaw, P. J. Oxidative stress in ALS: a mechanism of neurodegeneration and a therapeutic target. *Biochim. Biophys. Acta* **1762:**1051–1067; 2006.
[31] Barber, S. C.; Shaw, P. J. Oxidative stress in ALS: key role in motor neuron injury and therapeutic target. *Free Radic. Biol. Med.* **48:**629–641; 2010.
[32] Federico, A.; Cardaioli, E.; Da Pozzo, P.; Formichi, P.; Gallus, G. N.; Radi, E. Mitochondria, oxidative stress and neurodegeneration. *J. Neurol. Sci.* **322:**254–262; 2012.
[33] Ince, P.; Stout, N.; Shaw, P.; Slade, J.; Hunziker, W.; Heizmann, C. W.; Baimbridge, K. G. Parvalbumin and calbindin D-28k in the human motor system and in motor neuron disease. *Neuropathol. Appl. Neurobiol.* **19:**291–299; 1993.
[34] Alexianu, M. E.; Ho, B. K.; Mohamed, A. H.; La Bella, V.; Smith, R. G.; Appel, S. H. The role of calcium-binding proteins in selective motoneuron vulnerability in amyotrophic lateral sclerosis. *Ann. Neurol.* **36:**846–858; 1994.
[35] Reiner, A.; Medina, L.; Figueredo-Cardenas, G.; Anfinson, S. Brainstem motoneuron pools that are selectively resistant in amyotrophic lateral sclerosis are preferentially enriched in parvalbumin: evidence from monkey brainstem for a calcium-mediated mechanism in sporadic ALS. *Exp. Neurol.* **131:**239–250; 1995.
[36] Rothstein, J. D.; Tsai, G.; Kuncl, R. W.; Clawson, L.; Cornblath, D. R.; Drachman, D. B.; Pestronk, A.; Stauch, B. L.; Coyle, J. T. Abnormal excitatory amino acid metabolism in amyotrophic lateral sclerosis. *Ann. Neurol.* **28:**18–25; 1990.
[37] Rothstein, J. D.; Martin, L. J.; Kuncl, R. W. Decreased glutamate transport by the brain and spinal cord in amyotrophic lateral sclerosis. *N. Engl. J. Med.* **326:**1464–1468; 1992.
[38] Rothstein, J. D.; Van Kammen, M.; Levey, A. I.; Martin, L. J.; Kuncl, R. W. Selective loss of glial glutamate transporter GLT-1 in amyotrophic lateral sclerosis. *Ann. Neurol.* **38:**73–84; 1995.
[39] Trotti, D.; Rizzini, B. L.; Rossi, D.; Haugeto, O.; Racagni, G.; Danbolt, N. C.; Volterra, A. Neuronal and glial glutamate transporters possess an SH-based redox regulatory mechanism. *Eur. J. Neurosci.* **9:**1236–1243; 1997.
[40] Van Den Bosch, L.; Vandenberghe, W.; Klaassen, H.; Van Houtte, E.; Robberecht, W. Ca^{2+}-permeable AMPA receptors and selective vulnerability of motor neurons. *J. Neurol. Sci.* **180:**29–34; 2000.
[41] Vandenberghe, W.; Bindokas, V. P.; Miller, R. J.; Robberecht, W.; Brorson, J. R. Subcellular localization of calcium-permeable AMPA receptors in spinal motoneurons. *Eur. J. Neurosci.* **14:**305–314; 2001.

[42] Dykens, J. A. Isolated cerebral and cerebellar mitochondria produce free radicals when exposed to elevated Ca^{2+} and Na^{+}: implications for neurodegeneration. *J. Neurochem.* **63:**584–591; 1994.
[43] Carriedo, S. G.; Sensi, S. L.; Yin, H. Z.; Weiss, J. H. AMPA exposures induce mitochondrial Ca^{2+} overload and ROS generation in spinal motor neurons in vitro. *J. Neurosci.* **20:**240–250; 2000.
[44] Grosskreutz, J.; Van Den Bosch, L.; Keller, B. U. Calcium dysregulation in amyotrophic lateral sclerosis. *Cell Calcium* **47:**165–174; 2010.
[45] Mizushima, S.; Nagata, S. pEF-BOS, a powerful mammalian expression vector. *Nucleic Acids Res.* **18:**5322; 1990.
[46] Murai, K.; Murakami, H.; Nagata, S. Myeloid-specific transcriptional activation by murine myeloid zinc-finger protein 2. *Proc. Natl. Acad. Sci. USA* **95:** 3461–3466; 1998.
[47] Wang, J.; Slunt, H.; Gonzales, V.; Fromholt, D.; Coonfield, M.; Copeland, N. G.; Jenkins, N. A.; Borchelt, D. R. Copper-binding-site-null SOD1 causes ALS in transgenic mice: aggregates of non-native SOD1 delineate a common feature. *Hum. Mol. Genet* **12:**2753–2764; 2003.
[48] Witan, H.; Gorlovoy, P.; Kaya, A. M.; Koziollek-Drechsler, I.; Neumann, H.; Behl, C.; Clement, A. M. Wild-type Cu/Zn superoxide dismutase (SOD1) does not facilitate, but impedes the formation of protein aggregates of amyotrophic lateral sclerosis causing mutant SOD1. *Neurobiol. Dis.* **36:**331–342; 2009.
[49] Kramer-Albers, E. M.; Bretz, N.; Tenzer, S.; Winterstein, C.; Mobius, W.; Berger, H.; Nave, K. A.; Schild, H.; Trotter, J. Oligodendrocytes secrete exosomes containing major myelin and stress-protective proteins: trophic support for axons? *Proteomics Clin. Appl.* **1:**1446–1461; 2007.
[50] Spilker, C.; Gundelfinger, E. D.; Braunewell, K. H. Calcium- and myristoyl-dependent subcellular localization of the neuronal calcium-binding protein VILIP in transfected PC12 cells. *Neurosci. Lett.* **225:**126–128; 1997.
[51] Spilker, C.; Richter, K.; Smalla, K. H.; Manahan-Vaughan, D.; Gundelfinger, E. D.; Braunewell, K. H. The neuronal EF-hand calcium-binding protein visinin-like protein-3 is expressed in cerebellar Purkinje cells and shows a calcium-dependent membrane association. *Neuroscience* **96:**121–129; 2000.
[52] Permyakov, S. E.; Nazipova, A. A.; Denesyuk, A. I.; Bakunts, A. G.; Zinchenko, D. V.; Lipkin, V. M.; Uversky, V. N.; Permyakov, E. A. Recoverin as a redox-sensitive protein. *J. Proteome Res.* **6:**1855–1863; 2007.
[53] Olshevskaya, E. V.; Ermilov, A. N.; Dizhoor, A. M. Dimerization of guanylyl cyclase-activating protein and a mechanism of photoreceptor guanylyl cyclase activation. *J. Biol. Chem.* **274:**25583–25587; 1999.
[54] Vijay-Kumar, S.; Kumar, V. D. Crystal structure of recombinant bovine neurocalcin. *Nat. Struct. Biol.* **6:**80–88; 1999.
[55] Osawa, M.; Tong, K. I.; Lilliehook, C.; Wasco, W.; Buxbaum, J. D.; Cheng, H. Y.; Penninger, J. M.; Ikura, M.; Ames, J. B. Calcium-regulated DNA binding and oligomerization of the neuronal calcium-sensing protein, calsenilin/DREAM/KChIP3. *J. Biol. Chem.* **276:**41005–41013; 2001.
[56] Guo, Z.; Kozlov, S.; Lavin, M. F.; Person, M. D.; Paull, T. T. ATM activation by oxidative stress. *Science* **330:**517–521; 2010.
[57] Calabrese, V.; Guagliano, E.; Sapienza, M.; Panebianco, M.; Calafato, S.; Puleo, E.; Pennisi, G.; Mancuso, C.; Butterfield, D. A.; Stella, A. G. Redox regulation of cellular stress response in aging and neurodegenerative disorders: role of vitagenes. *Neurochem. Res.* **32:**757–773; 2007.
[58] Calabrese, V.; Cornelius, C.; Dinkova-Kostova, A. T.; Iavicoli, I.; Di Paola, R.; Koverech, A.; Cuzzocrea, S.; Rizzarelli, E.; Calabrese, E. J. Cellular stress responses, hormetic phytochemicals and vitagenes in aging and longevity. *Biochim. Biophys. Acta* **1822:**753–783; 2012.
[59] Rattan, S. I. The nature of gerontogenes and vitagenes: antiaging effects of repeated heat shock on human fibroblasts. *Ann. N. Y. Acad. Sci.* **854:**54–60; 1998.
[60] Calabrese, V.; Cornelius, C.; Cuzzocrea, S.; Iavicoli, I.; Rizzarelli, E.; Calabrese, E. J. Hormesis, cellular stress response and vitagenes as critical determinants in aging and longevity. *Mol. Aspects Med.* **32:**279–304; 2011.
[61] Fierro-Gonzalez, J. C.; Gonzalez-Barrios, M.; Miranda-Vizuete, A.; Swoboda, P. The thioredoxin TRX-1 regulates adult lifespan extension induced by dietary restriction in *Caenorhabditis elegans*. *Biochem. Biophys. Res. Commun.* **406:**478–482; 2011.
[62] Calabrese, V.; Cornelius, C.; Stella, A. M.; Calabrese, E. J. Cellular stress responses, mitostress and carnitine insufficiencies as critical determinants in aging and neurodegenerative disorders: role of hormesis and vitagenes. *Neurochem. Res.* **35:**1880–1915; 2010.
[63] Ames, J. B.; Porumb, T.; Tanaka, T.; Ikura, M.; Stryer, L. Amino-terminal myristoylation induces cooperative calcium binding to recoverin. *J. Biol. Chem.* **270:**4526–4533; 1995.
[64] Ladant, D. Calcium and membrane binding properties of bovine neurocalcin delta expressed in Escherichia coli. *J. Biol. Chem.* **270:**3179–3185; 1995.
[65] Tanaka, T.; Ames, J. B.; Harvey, T. S.; Stryer, L.; Ikura, M. Sequestration of the membrane-targeting myristoyl group of recoverin in the calcium-free state. *Nature* **376:**444–447; 1995.
[66] Williams, T. A.; Monticone, S.; Crudo, V.; Warth, R.; Veglio, F.; Mulatero, P. Visinin-like 1 is upregulated in aldosterone-producing adenomas with KCNJ5 mutations and protects from calcium-induced apoptosis. *Hypertension* **59:**833–839; 2012.
[67] Roy, N.; Mahadevan, M. S.; McLean, M.; Shutler, G.; Yaraghi, Z.; Farahani, R.; Baird, S.; Besner-Johnston, A.; Lefebvre, C.; Kang, X.; et al. The gene for neuronal apoptosis inhibitory protein is partially deleted in individuals with spinal muscular atrophy. *Cell* **80:**167–178; 1995.
[68] Mercer, E. A.; Korhonen, L.; Skoglosa, Y.; Olsson, P. A.; Kukkonen, J. P.; Lindholm, D. NAIP interacts with hippocalcin and protects neurons against calcium-induced cell death through caspase-3-dependent and -independent pathways. *EMBO J.* **19:**3597–3607; 2000.
[69] Lindholm, D.; Mercer, E. A.; Yu, L. Y.; Chen, Y.; Kukkonen, J.; Korhonen, L.; Arumae, U. Neuronal apoptosis inhibitory protein: structural requirements for hippocalcin binding and effects on survival of NGF-dependent sympathetic neurons. *Biochim. Biophys. Acta* **1600:**138–147; 2002.
[70] Calabrese, V.; Cornelius, C.; Dinkova-Kostova, A. T.; Calabrese, E. J.; Mattson, M. P. Cellular stress responses, the hormesis paradigm, and vitagenes: novel targets for therapeutic intervention in neurodegenerative disorders. *Antioxid. Redox Signaling* **13:**1763–1811; 2010.
[71] Cohen, T. J.; Hwang, A. W.; Unger, T.; Trojanowski, J. Q.; Lee, V. M. Redox signalling directly regulates TDP-43 via cysteine oxidation and disulphide cross-linking. *EMBO J.* **31:**1241–1252; 2012.
[72] Jheng, F. F.; Wang, L.; Lee, L.; Chang, L. S. Functional contribution of Ca^{2+} and Mg^{2+} to the intermolecular interaction of visinin-like proteins. *Protein J.* **25:**250–256; 2006.
[73] Karch, C. M.; Prudencio, M.; Winkler, D. D.; Hart, P. J.; Borchelt, D. R. Role of mutant SOD1 disulfide oxidation and aggregation in the pathogenesis of familial ALS. *Proc. Natl. Acad. Sci. USA* **106:**7774–7779; 2009.
[74] Youn, H.; Jeoung, M.; Koo, Y.; Ji, H.; Markesbery, W. R.; Ji, I.; Ji, T. H. Kalirin is under-expressed in Alzheimer's disease hippocampus. *J. Alzheimers Dis.* **11:**385–397; 2007.
[75] Lee, J. M.; Blennow, K.; Andreasen, N.; Laterza, O.; Modur, V.; Olander, J.; Gao, F.; Ohlendorf, M.; Ladenson, J. H. The brain injury biomarker VLP-1 is increased in the cerebrospinal fluid of Alzheimer disease patients. *Clin. Chem.* **54:**1617–1623; 2008.
[76] Tarawneh, R.; D'Angelo, G.; Macy, E.; Xiong, C.; Carter, D.; Cairns, N. J.; Fagan, A. M.; Head, D.; Mintun, M. A.; Ladenson, J. H.; Lee, J. M.; Morris, J. C.; Holtzman, D. M. Visinin-like protein-1: diagnostic and prognostic biomarker in Alzheimer disease. *Ann. Neurol.* **70:**274–285; 2011.
[77] Luo, X.; Hou, L.; Shi, H.; Zhong, X.; Zhang, Y.; Zheng, D.; Tan, Y.; Hu, G.; Mu, N.; Chan, J.; Chen, X.; Fang, Y.; Wu, F.; He, H.; Ning, Y. CSF levels of the neuronal injury biomarker visinin-like protein-1 in Alzheimer's disease and dementia with Lewy bodies. *J. Neurochem.* **127:**681–690; 2013.